Journal of
Materials Chemistry B

ROYAL SOCIETY
OF CHEMISTRY

REVIEW

View Article Online
View Journal | View Issue

Cite this: *J. Mater. Chem. B*, 2025, **13**, 10420

Received 1st May 2025,
Accepted 1st August 2025

DOI: 10.1039/d5tb01040c

rsc.li/materials-b

Graphene-based neural electrodes: from materials and device fabrication to properties

Muhammed Zahid Doğan[a] and Cem Bayram *[ab]

Neural electrodes serve as a conduit for the purpose of facilitating electrophysiological communication between neurons and external electronic devices. These electrodes are extensively utilized in both neuroscientific research and in the domains of neural prosthetics and neuromodulation practices. Recently, graphene and its numerous derivatives have emerged as a transformative material in bioelectronics and electrochemical applications. Depending on the device fabrication process and preferred graphene derivative, graphene-based neural electrodes can offer fatigue-resistant flexibility, high electrical conductivity, excellent optical transparency (97.7%), increased specific surface area, superior electrochemical durability, composability, and advanced surface functionalization properties, which can make them an ideal choice for their intended *in vivo* or *in vitro* applications. In this review, we comparatively summarize the existing work on graphene and graphene related material-based electrochemical neural electrodes through the key studies of diverse approaches to provide an overview of the field, highlight the motivations behind the research, and identify potential improvement strategies for future investigations.

1. Introduction

Neurons are electrical cells that can experience a modulation of their membrane potential in response to chemical, mechanical, optical and electrical stimulations.[1] In addition, neurons can transmit the information they receive through synaptic communication with other cells by forming action potentials, which are initiated when the neuron receives sufficient stimulation to create a potential difference that exceeds the membrane threshold potential.[1,2] Bridging bidirectional electrophysiological communication between neurons and external electronics, neural electrodes are indispensable tools for neuroscience studies, as well as for neural prostheses and neuromodulation devices that offer significant practical benefits in the diagnosis and treatment of hearing loss, visual impairment, epilepsy, and Parkinson's disease.[3] Recent advancements in computational power and signal processing techniques have rendered it possible to process

---

[a] *Hacettepe University, Graduate School of Science and Engineering, Department of Nanotechnology and Nanomedicine, Ankara, Türkiye. E-mail: cemb@hacettepe.edu.tr*

[b] *Hacettepe University, Advanced Technologies Application and Research Centre, Ankara, Türkiye*

Muhammed Zahid Doğan

Muhammed Zahid Doğan graduated in Electrical and Electronics Engineering at Gazi University, Turkey, in 2019. He received his master's degree in Nanotechnology and Nanomedicine from Hacettepe University in 2023 and is currently pursuing a PhD degree in the same department. His current research interests include nanotechnological applications in chemical sensors, bioelectronics, and surface bioengineering.

Cem Bayram

Cem Bayram is a professor at the Nanotechnology and Nanomedicine Department at Hacettepe University. His research focuses on biomaterials and bottom-up biofabrication technologies and involves co-researchers from various fields, including basic sciences, engineering, medicine, pharmacy, and dentistry.

large amounts of neural recording data and generate independent multi-electrode stimulation patterns. Consequently, there is an increasing momentum in neural electrode studies to develop high-performance interfaces for both *in vivo* and *in vitro* applications.[4,5] Multidisciplinary approaches are currently being employed in the fields of materials science, electronics, and bioengineering to engineer advanced electrodes that exhibit high spatial resolution and chronic stability. The development of these electrodes necessitates the utilization of superior materials with enhanced electrochemical performance. The objective is to facilitate the recording of the complex dynamics of neural activity through weak electrophysiological signals, while concurrently enabling effective manipulation of the neural system.[6,7]

Unlike non-invasive electroencephalography (EEG) and patch-clamp electrodes that interact with the cell membrane, electrocorticography (ECoG) electrodes placed over the cortex, as well as intracortical and deep brain stimulation electrodes placed within the cortex, communicate with targeted neurons through extracellular fluid interactions.[5,8] In conjunction with electrode arrays utilized in *in vitro* cell experiments, these electrochemically interacting electrodes facilitate reduced external noise and the capacity to electrically stimulate neural cells and tissues.[9–11] The mechanical and chemical compatibility of these electrodes and their substrates with the surrounding viscoelastic matrix is crucial for effective electrical connection to the target cells. Such compatibility preserves the viability of neurons around the device while also preventing the electrodes from being surrounded by electrically insulating astrocyte cells which are formed as a result of wounding and neuroinflammatory responses.[10,12,13] In addition to improvements in biocompatibility, scaling down the size of extracellular electrodes to micro dimensions for high-precision recording and stimulation capabilities remains a topic of great interest among researchers in the field. However, the reduction in electrode size also leads to a significant increase in the electrochemical interface impedance of the electrode, resulting in attenuation and elevated thermal noise contribution in the acquired signals.[4,5] Moreover, the elevated impedance exhibited by microelectrodes imposes a substantial constraint on the maximum amplitude of current that can be safely applied by the electrode.[4,7]

Conventional methodologies and materials employed in the fabrication of neural microelectrodes, such as the deposition of noble metals or ceramic materials (*e.g.*, platinum, gold, and titanium nitride [TiN]) on rigid silicon substrates utilizing standard microfabrication techniques, are proving to be inadequate in meeting the current demands and challenges.[13–16] Consequently, there has been a surge in research focusing on innovative designs and nanomaterials featuring decreased impedance per unit geometric surface area (GSA), alongside flexibility, biocompatibility, robustness, and multimodal capabilities.[9–11,17,18] In this sense the bending stiffness (eqn (1)) parameter is considered to be a critical factor[19,20] for ensuring the mechanical compatibility of devices with the neural tissue which is characterized by a modulus of linear elasticity in the range of 100 Pa to 10 kPa.[19] In the present literature, ultrathin films of inert polymers suitable for photolithography such as polyimide (PI), parylene, and polyethylene terephthalate are used as substrates to fabricate biocompatible and low bending stiffness neural probes.[9,21,22] The utilization of transparent polymer substrates facilitates the exploitation of multimodal capabilities, such as multiphoton microscopy and optogenetic stimulation, in conjunction with electrophysiological measurements.[23] Coupled with the transparent substrates, the employment of optically transparent materials within the electrode regions has been demonstrated to further eliminate light-induced artefacts and therefore enable greater reliability and precision in sophisticated measurement and manipulation operations.[17,24,25]

$$D = \frac{Eh^3}{12(1 - \nu^2)} \tag{1}$$

Eqn (1) flexural rigidity (bending stiffness (D)) of a thin plate, where E is the elastic modulus of the material, h is the thickness, and ν is the Poisson's ratio.

Since its discovery in 2004, intensive studies have revealed the unique properties and alternative manufacturing methods of graphene, which is essentially a two-dimensional honeycomb network of carbon. The employment of a range of production techniques results in the generation of graphene in diverse forms, including mono/few-layer graphene, graphene oxide (GO), reduced graphene oxide (rGO), graphene nanoplatelets (GNP), and laser-induced porous graphene (LIG). Collectively, these materials are categorized as ''graphene-related materials'' (GRM). The selection of the optimal form for the intended application results in the acquisition of graphene-based neural electrodes, which possess a range of advantageous characteristics. These include high electrical conductivity, high optical transparency (97.7%), outstanding MRI compatibility, enhanced electrochemical surface area, improved mechanical strength, electrochemical durability, composability, economic viability and enhanced surface functionalization capabilities. In addition to these properties, electrodes made of graphene with low electrode layer thickness ($\sim$0.3 nm to 3 nm) and GRM-based materials consisting of micro-nano-sized particles offer flexible application possibilities for free-standing and thin-film coated neural electrodes. In this review, the electrochemical evaluation methods of neural electrodes are first introduced in a concise manner. In this review, we first provide a brief introduction to the electrochemical evaluation methods of neural electrodes. Thereafter, a summary of existing work on graphene and graphene-related material-based electrochemical interfaces for neural electrodes is presented through key studies to provide an overview of the field, highlight the motivation behind the studies, and identify potential improvement strategies for future research.

2. Electrochemical evaluation of graphene neural electrodes

In comparison to non-invasive techniques, neural electrodes that interact directly with the extracellular matrix in intracranial, intracortical and *in vitro* approaches offer high-quality recordings and precise stimulation due to the close contact with target cells. However, they also introduce new parameters and design constraints that must be considered when developing electrodes. In order to establish an electrical connection with neurons targeted by these electrodes, it is necessary to ensure that the solid–liquid interface, where the electronic current is converted into an ionic current and *vice versa*, is composed of biocompatible materials that are also resilient to mechanical failure factors, such as corrosion, delamination and dissolution of electrode and the swelling of hydrophilic based interfaces, for years and under a continuous electrical load.[4]

In addition to the invasive/non-invasive distinction, the literature further classifies the invasive electrochemical neural electrodes into two groups with respect to their geometric surface area (GSA). Neural electrodes that exhibit an advantage in terms of size reduction and that establish close contact with neurons to enhance spatial resolution (typically with an average GSA of less than 100 000 μm^2) are designated as microelectrodes. Conversely, electrodes of a greater size are categorized as macroelectrodes.[5] The voltage (V) produced by an current (I) in the electrolyte at a distance "r" from the source is expressed as: $V = I/4\pi\sigma r$, where "σ" is representing the conductivity of the medium (1–2 S m^{-1}).[13] While the equation emphasizes the influence of electrode distance on signal attenuation, experimental and theoretical studies have shown that interface impedance plays a decisive role in electrode performance, particularly for microelectrodes as demonstrated in Fig. 1.[4,5,14,26,27] The high impedance of the interface reduces the potential received by the amplifier device in recording applications, making the signal more susceptible to external noise and additionally reduce the signal-to-noise ratio (SNR) by introducing thermal noise.[4,14,28]

During stimulation applications, the delivery of current to the target region through a high interface impedance result in an increased voltage drop across the electrode interface. This, in turn, can induce irreversible chemical reactions. Reactions of this kind are known to result in electrode degradation and the release of toxic reactive species. Therefore, it is important to limit the peak stimulation current delivered by the electrode to a range that does not exceed the safe interfacial voltage limits of the material.[7] The conventional approach to determining the safe voltage range of neural electrodes involves the ascertainment of the lower and upper boundary potentials. The limits in question are defined as the boundaries that delineate the absence of reduction or oxidation of water in an electrolyte exhibiting an ionic content analogous to that of neural media[4,28–30] (Fig. 2a). The upper and lower limits of this range, also known as "the water window", are usually determined by researchers through analysis of cyclic voltammetry (CV) scans.[5] In a typical procedure, multiple CV measurements are taken by expanding the potential range of the scans in each iteration, and threshold potentials are identified at the onset of water splitting reactions observed by prominent current peaks.

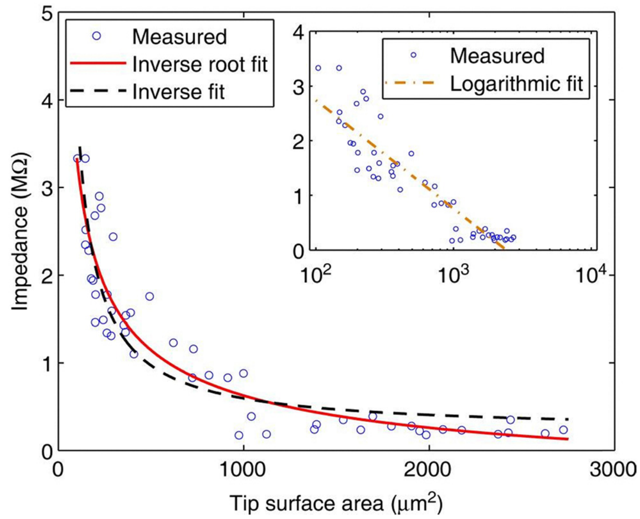

Fig. 1 Experimental demonstration of the sudden rise in the electrochemical impedance of electrodes at microscale dimensions. Reproduced from ref. 27 with permission from Frontiers, Copyright 2009.

Following the identification of the tolerable voltage range, an investigation of neural stimulation capability of the electrode conducted either directly through the measurement of the maximum transferable charge in the leading phase of the "biphasic charge balanced signal" or indirectly through the calculation of the charge storage capacity (CSC), which provides a practical way for prediction of electrode stimulation capability based on CV measurements[4,7] (Fig. 2b). As the cathodic phase is generally considered the optimal leading phase of stimulation due to electrochemical safety reasons,[5] it is also a common practice to characterize electrodes based on the area enclosed by the negative half cycle of the CV scan (CSC_c).[5] On the other hand, the maximum leading phase charge, also known as the charge injection capacity (CIC), has been identified as a robust and application-oriented parameter that has been used in numerous comprehensive studies for the characterization of neural electrodes.[25,31–34] The quantification of the CIC necessitates the employment of high-speed data acquisition systems for the analysis of the transient voltage response with respect to the applied current, for the determination of electrode potential excursions beyond the water window. In return, this fulfils a crucial role in neural stimulation applications by defining the upper limit of safely injectable currents for distinct phase durations (Fig. 2c). It is therefore evident that the accuracy of CIC measurements, as well as the validity of data obtained by the aforementioned methods, is contingent upon the alignment of experimental parameters with the current frequency of the desired neural application conditions.[5]

As a convenient and versatile tool, researchers also benefit from electrochemical impedance spectroscopy (EIS) measurements and associated equivalent circuits. These measurements and circuits are used for the practical evaluation of electrode performance, charge transfer characteristics and the validation of CSC-CIC results (Fig. 3 and 4). In the context of EIS analysis, the impedance spectrum of the system, encompassing the neural electrode, electrolyte, and counter electrode, is derived through the magnitude and phase angle of the current generated between the

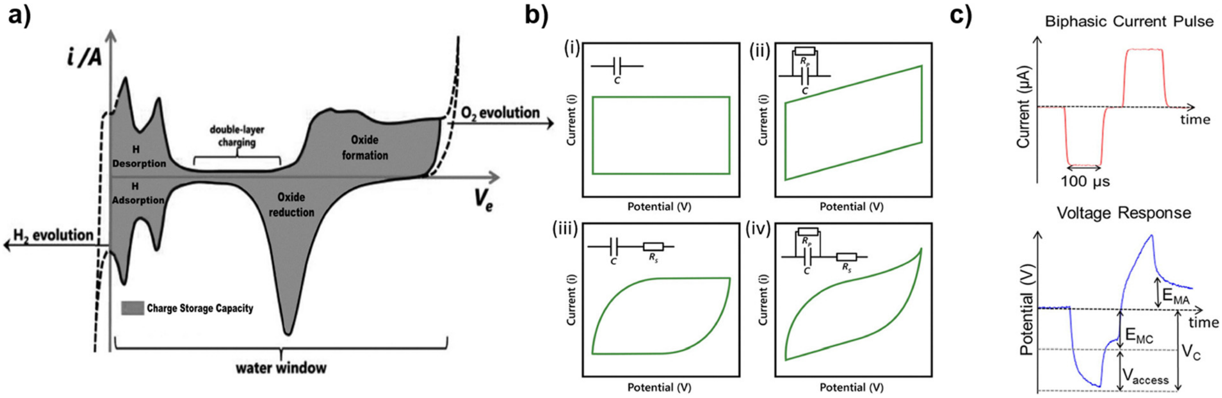

Fig. 2 The determination of water window and the CSC area by setting limits prior O_2 (anodic) and H_2 (cathodic) evolution (a). Adapted from ref. 35, with permission from Wiley, Copyright 2021. Alterations of CV profile based on the dominating charge transfer characteristics of electrode (b). Reproduced from ref. 36, with permission from Wiley, Copyright 2021. Measurement of CIC *via* biphasic current application and identification of potential drop on the electrode interface (c). Reproduced from ref. 37, with permission from Frontiers, Copyright 2015.

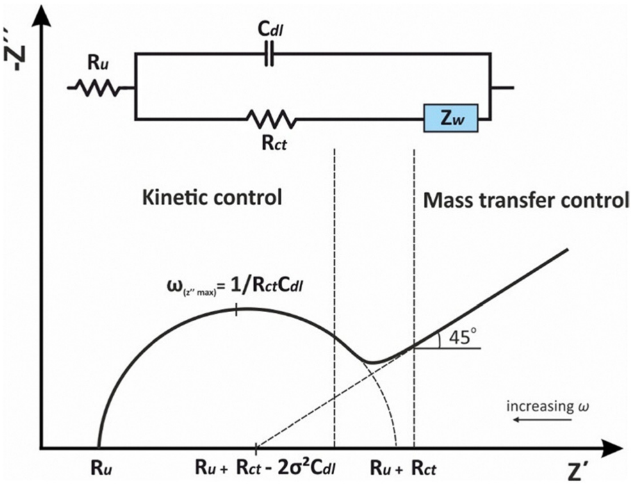

Fig. 3 The EIS bode plot and corresponding Randles circuit including solution resistance R_u, double layer capacitance C_{dl}, charge transfer resistance R_{ct} and the Warburg Z_w element to represent mass transfer limitations. Reproduced from ref. 38, with permission from American Chemical Society, Copyright 2023.

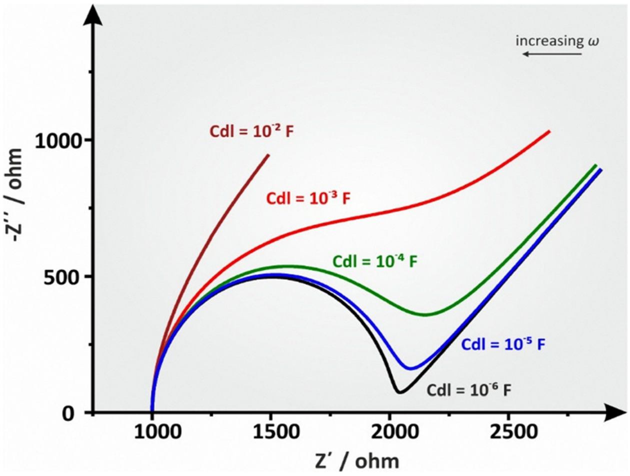

Fig. 4 Change in the EIS profile as a result of increasing electrode capacitance, with other parameters held constant. Reproduced from ref. 38, with permission from American Chemical Society, Copyright 2023.

neural electrode and the counter electrode. This is achieved by application of sinusoidal signals of varying frequencies individually to the neural electrodes, with amplitudes ranging from 10 to 100 millivolts. These low signal levels are deliberately chosen to ensure that there is no irreversible reaction occurring.[4]

Reliable and accurate measurement of the neural electrode requires minimizing the interference from electrolyte and counter electrode impedances that are connected in series with the neural electrode and consequently contributing to the final impedance of the system. In order to ascertain the electrolyte's share on total impedance, researchers adopted a straightforward solution, namely to reduce the distance between the electrodes. Keeping the size of the neural electrode significantly smaller than the counter electrode is also considered as a good practice that increases the contribution of neural electrode to the overall impedance of the system and ensures that the measurement reflects the true characteristic of the neural electrode.[5] In a similar way, keeping the surface roughness of the tested electrode the same as the microelectrode in applications provides an accurate reflection of the neural electrode surface by not changing the electrochemical surface area (ESA) per GSA.

The aforementioned electrochemical characterization methods have been also utilized to assess the long-term stability of neural electrodes produced through various manufacturing techniques, coatings, composites, chemical modifications, and flexibility features that can significantly impact their durability under environmental and operating conditions. While 1× phosphate-buffered saline (PBS) electrolyte is often used as a reference of brain extracellular fluid[39,40] for simulation of environmental conditions, the addition of H_2O_2 to solution, in conjunction with increased temperature, also been adopted to accelerate aging process.[41,42] These cell-free stability assays can be carried out by performing compelling tasks such as prolonged electrolyte soaking, multiple CV scans, or biphasic stimulations.[15,33,43–45] Researchers often evaluated the electrode stability based on the percentage reduction in CSC value of CV scans or the increase in impedance observed at the once broadly accepted but currently controversial[4,28] 1 kHz perturbation signal. Beside the mentioned cell-free methods, comprehensive studies also benefit from cell culture and animal assays that truly resembles the external factors of the application environment where pH, oxygen density and conductivity of medium are dynamically altering by the presence of nutrients & metabolites, protein adsorption, electrode biofouling, tissue anisotropy, and the immune system response.[4,6,29,46,47]

Considering these reference points, identifying the electrochemical parameters of neural electrodes—and examining how they vary under specific conditions—offers the research community a convenient, comprehensive, and widely accepted approach for evaluating electrodes across multiple dimensions.

3. Utilization of graphene and graphene related materials in neural electrodes

3.1. CVD graphene

A considerable number of studies have been conducted over the past decade, employing single and multilayer graphene obtained through the chemical vapor deposition (CVD) method for research into neural electrodes.[15,21,25,31,32,48–55] During this period, CVD graphene emerged a major branch for graphene based neural electrode studies (Fig. 5) as it offers the best of both worlds compared to existing flat electrodes such as platinum, gold, and TiN, which have robust electrical and electrochemical properties but are limited in terms of transparency and flexibility, and novel electrodes made from indium tin oxide and conductive polymers, which are limited in terms of either flexibility or optical transparency.

The inherent nature of CVD graphene thus motivates researchers to use graphene with varying numbers of layers and to explore novel surface modification strategies in neural electrode studies. In particular, the balance between repeatable electrode performance and higher optical transparency *versus* the potential severity of transfer errors, increased sheet resistance, and reduced operational reliability are critical considerations in minimizing the number of CVD graphene layers to be used as neural electrodes.[31,53] A further challenging aspect that emerges from the extant literature is the reduction of the electrochemical impedance, which is considerably higher than that of metals and conductive polymers. The high impedance is mainly caused by two factors, firstly the limited ESA/GSA ratio of flat graphene surfaces and secondly the reduced faradaic reaction sites due to the high crystallinity of inert electrode.[4,5,50] Consequently, the researchers are also investigating ways to enhance the electrochemical efficiency of the existing electrode surfaces of CVD graphene electrodes.

In this regard, the research published by Kuzum *et al.* in 2014[15] holds a significant importance, as it represents one of the earliest studies in the field and underscores the essential aspects. In the study, 50 × 50 μm^2 neural electrodes formed by wet transfer of CVD graphene onto 25 μm thick PI substrates and subsequent photolithographic patterning, were used for simultaneous optical and electrophysiological recording of neurons both *in vitro* and *in vivo*. Moreover, the authors indicate a reduction in the electrochemical impedance values and an increase in the CSC of the electrodes (Table 1) as a consequence of the p-type doping of graphene through electropositive NO_3^- adsorption[15] and/or, more likely, the formation of reactive sites by newly formed defects resulting from acid treatment. This assumption is further corroborated by the EIS phase angle results, which demonstrate that the EIS phase angles of the doped graphene electrodes exhibit notable differences at specific scan rates in comparison to the undoped graphene electrodes and the observed difference can be attributed to the altering electrochemical reaction kinetics.[36]

The study demonstrated that single cell recording can be achieved with graphene electrodes as well as with gold electrodes measuring 500 × 500 μm^2, which were created for control purposes. In addition, the researchers noted that the impedance of the doped graphene electrodes exhibited comparable values to those of the gold electrodes at 1 kHz however demonstrated a six times lower root-mean-square (RMS) noise. Meanwhile, the undoped graphene electrodes exhibited considerably elevated impedance and demonstrated noise in between the gold and doped graphene electrodes. Whilst the present results lend support to the aforementioned[4,28] concerns regarding the validity of the 1 kHz impedance, the authors have also indicated the potential for a limited

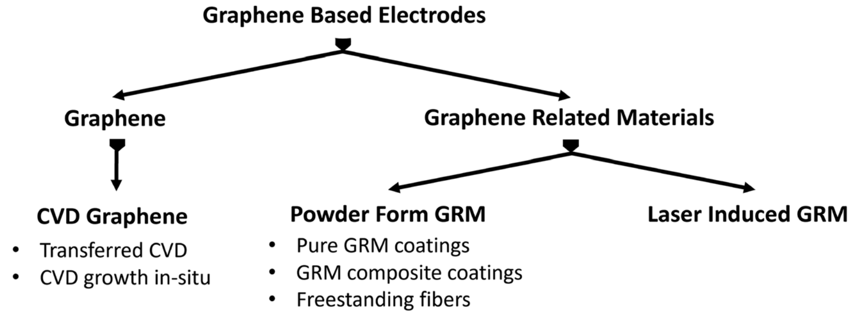

Fig. 5 Overview of major research branches in graphene-based neural electrodes from the current literature.

Table 1 Summary of electrochemical characterizations reported in CVD graphene studies

Materials	Impedance @ 1 kHz	CSC	CIC	SNR	Electrode size	Ref.
Gold	17.2 kΩ (500 × 500 µm)	0.402 mC cm^{-2} (200 mV s^{-1})	—	7.7 (500 × 500 µm)	50 × 50 and 500 × 500 µm	15
Plain graphene	—	0.735 mC cm^{-2} (200 mV s^{-1})	—	—	50 × 50 µm	
HNO$_3$ doped graphene	541 kΩ	1.953 mC cm^{-2} (200 mV s^{-1})	—	40.8	50 × 50 µm	
Graphene	4.03 MΩ	—	—	—	100 × 100 µm	24
Graphene (4SCM applied)	963 kΩ	—	—	—	100 × 100 µm	
Graphene	872.9 kΩ	—	—	—	100 × 100 µm	22
PtNP & Graphene (5–50 s)	∼(100 k–10 kΩ)	—	—	—	100 × 100 µm	
Graphene (4 layer)	286 kΩ	—	57.13 µC cm^{-2} 116.07 µC cm^{-2}[a]	—	∅ 100 µm	25
Graphene (multi-layer)	27 kΩ	2.42 mC cm^{-2} (200 mV s^{-1})	44 µC cm^{-2}		∅ 340 µm (295 µm[b])	31
Graphene (2 layer-HNO$_3$ & PtNP)	200 kΩ	30.72 mC cm^{-2} ([c])	—	—	∅ 20 µm	55
Gold	2.65 MΩ	0.73 mC cm^{-2} (1 V s^{-1})	0.16 mC cm^{-2}	—	∼700 µm^2	48
Graphene	1.08 MΩ	0.91 mC cm^{-2} (1 V s^{-1})	0.15 mC cm^{-2}	35.8	∼700 µm^2	
Graphene coated gold	860 kΩ	1.58 mC cm^{-2} (1 V s^{-1})	0.31 mC cm^{-2}	66.6	∼700 µm^2	
Circular Pt	∼130 kΩ	∼4.5 mC cm^{-2} (50 mV s^{-1})	∼0.20 mC cm^{-2}	—	7854 µm^2	32
Fractal Pt	∼50 kΩ	∼7.5 mC cm^{-2} (50 mV s^{-1})	∼0.75 mC cm^{-2}	—	7854 µm^2	
Graphene coated circular Pt	∼350 kΩ	∼3 mC cm^{-2} (50 mV s^{-1})	∼0.20 mC cm^{-2}	—	7854 µm^2	
Graphene coated fractal Pt	∼75 kΩ	∼4 mC cm^{-2} (50 mV s^{-1})	∼0.75 mC cm^{-2}	—	7854 µm^2	

[a] With failure benchmark test. [b] After subtraction of the hole areas on the electrode surface. [c] Unspecified scan rate.

contribution of thermal noise in comparison to biological and other noise factors. The study further demonstrated that the obtained electrophysiological recordings during confocal and multiphoton microscopy using the graphene electrode arrays exhibited clear signals without the light-induced artefacts which were evident for the metal electrodes as a consequence of the photoelectric effect.

In the subsequent years, the findings of this study were incorporated into another investigation, and the impact of crack formation and organic residues which capable of generating photovoltaic and photothermal currents was further mitigated by employing a meticulous fabrication process. Advancements of this kind have paved the way for the remarkable accomplishment of achieving crosstalk-free optogenetic excitation, two-photon imaging, and electrical recording in a single experiment on CVD graphene neural electrodes.[24] The process was optimized through the implementation of several techniques, including the utilization of bubble transfer[56] for the peeling of graphene from its growth metal without the necessity of etching, which could potentially result in graphene contamination. Additionally, the conventional photoresist was substituted with polymethyl glutarimide (PMGI) in the electrode patterning process, leading to a reduced amount of residual material after removal. The authors further developed a 4-step stripping/cleaning method (4SCM) that results in efficient removal of artifact-inducing photoresists, combined with a significant reduction in electrochemical impedance and minimization of inter-electrode impedance variation (Fig. 6). Researchers also reported that the graphene electrodes achieved precise imaging to a depth of 1200 µm using deep two-photon imaging on the surface of primary somatosensory cortex without suffering from any electrode-induced obstacles. Taken together, the findings of this study not only exemplify the high potential of bare CVD graphene electrodes but also demonstrate the significant impact of optimizing fabrication conditions on device performance.

Beside optoelectronic enhancements, studies are also aimed to improve the stability and performance of electrophysiological recording and stimulation capabilities present in CVD-based graphene electrodes. Lu *et al.*[22] experimentally demonstrated that the "quantum capacitance" phenomenon[57] resulting from the unique structure of graphene in overcoming the high electrochemical impedance of these electrodes. The quantum capacitance effect was studied using equivalent circuits obtained from impedance measurements of pristine electrodes in 1× PBS electrolyte. In these measurements, the calculated double layer capacitance (C_{dl}) was reported to be 7.07 µF cm^{-2}, and the quantum capacitance, modeled in the equivalent circuit as being in series with C_{dl}, was reported to be 2.45 µF cm^{-2}, both with low interelectrode standard deviations. The authors emphasize the detrimental impact of the low quantum capacitance in series with the double layer capacitance on the overall capacitive current path of the electrode. Rather than the chemical doping of graphene, which shifts the Fermi level away from the Dirac point with minimal effect[58] and causes graphene to still exhibit a significant quantum capacitance effect, an alternative redox pathway is considered, involving the deposition of platinum nanoparticles (PtNP) onto the electrode surface to reduce the overall impedance. Accordingly, different densities of PtNP electrodeposition were explored on the electrode surfaces by varying the deposition time, and up to 100-fold reduction in total impedance was achieved (Fig. 7). The modified electrodes were then

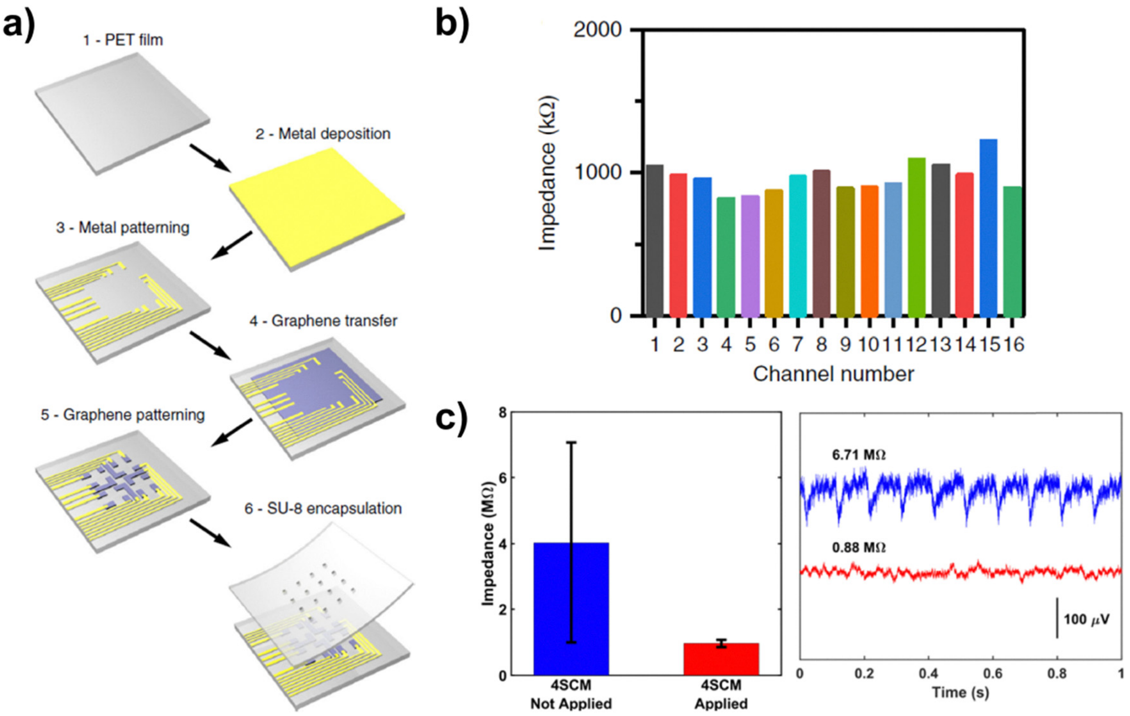

Fig. 6 The general fabrication steps of graphene microelectrode array, where 4SCM is employed in the residue removal phase of the graphene patterning (5) process (a). The uniform inter-channel impedance levels of the obtained electrode array (b). Comparison of graphene electrodes with and without 4SCM process: left, 1 kHz impedance levels of electrodes and right, the resulting illumination-induced artifact potentials generated at 470 nm wavelength exposure (c). Reproduced from ref. 24, with permission from Nature, Copyright 2018.

subjected to two-photon *in vivo* calcium imaging, and no adverse effects on the images were reported. Although this modification offers low electrochemical impedance (Table 1) without affecting optical applications, it's also important to consider the corrosion susceptibility of PtNP and the stability of its bond with the graphene surface[59] especially for use in long-term applications.

The evaluation of multilayer CVD graphene neural electrodes for the improvement of electrophysiological measurements has also been explored in studies.[21,25,31] The employment of multilayer graphene functions as an auxiliary safety measure, the purpose of which is to avert the repercussions of defects on the fragile monolayer graphene surface. These defects have the potential to result in channel loss or substantial inter-electrode impedance variations. On the other hand multilayered graphene can also reduce the sheet resistance and electrochemical impedance of the electrodes.[25,31] In the papers published in 2014 and 2018, Park *et al.* conducted detailed investigations of the devices fabricated by stacking four individual single-layer graphene sheets based on the carbon-layer electrode array (CLEAR) protocol developed by the research group.[21,25,60] The implementation of 4-layer graphene resulted in a significant reduction of the electrode sheet resistance with a decrease from 152 Ω to 76 Ω per square while maintaining 90% transmittance over the infrared to ultraviolet spectrum. However, light-induced artifacts in optogenetic applications have been reported to be observed with an amplitude comparable to that of the platinum electrodes. The CIC measurement of CLEAR electrodes performed in accordance with the literature determined a charge density of 57.13 μC cm^{-2} as the stimulation limit and in addition, authors stated that safe stimulation can be performed using a charge density up to 116.07 μC cm^{-2} under the so-called "Failure benchmark test", which refers to the interpretation of whether failure occurs at the applied current by analyzing the change in electrode's electrochemical impedance.[25]

In the article published in 2022, Babaroud *et al.* developed a multilayer graphene electrode fabrication process that circumvents the challenges associated with manual graphene transfer and facilitates wafer-scale device fabrication (Fig. 8).[31] The process is initiated by the CVD growth of graphene on a 50 nm-thick molybdenum template that has been previously deposited and patterned as an electrode array on a SiO_2 substrate. In the subsequent stage, the graphene-coated electrode array is to be covered by a new polymer substrate, with the deposition of parylene C and the patterning of the electrode sites on the polymer. Finally, the etching of the molybdenum template is performed on the reverse side, and the graphene layer is sandwiched by a second deposition of parylene C. The study reported that no light-induced artefacts were observed in any of the multilayer graphene (MLG) of different thicknesses as a result of the fabrication of MLG electrodes without contamination of transfer polymer and the absence of transfer-induced defects. However, the fabrication method used in this study requires the formation of holes without graphene on the electrode surface (Fig. 8b), which compromises the device's electrochemical performance per unit area (Table 1).

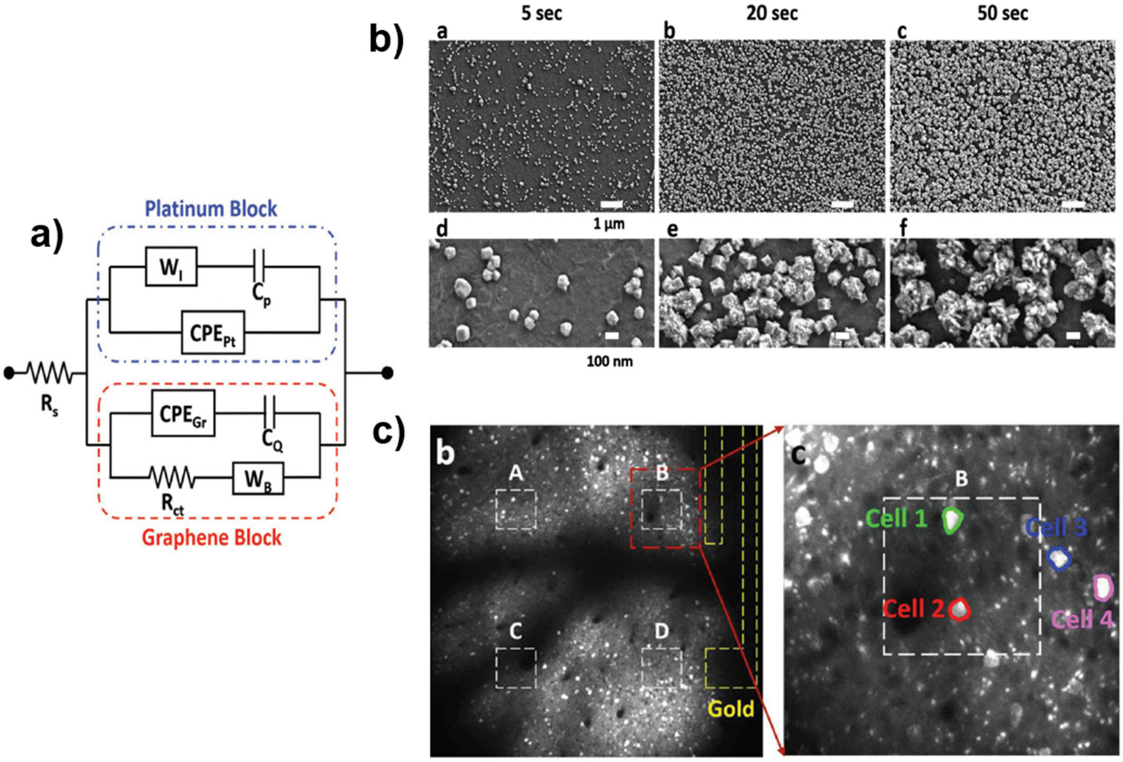

Fig. 7 The new equivalent circuit model of the graphene-PtNP hybrid surface after the introduction of platinum NP (a). SEM images of 5, 20, 50 seconds of PtNP deposition (b) and the optical effect of the deposition duration on the two photon images (left) and optical ability demonstration of the most densely coated graphene sample (A, B, C and D are 10, 50, 5 and 5 seconds respectively) (c). Reproduced from ref. 22 with permission from John Wiley and Sons, Copyright 2018.

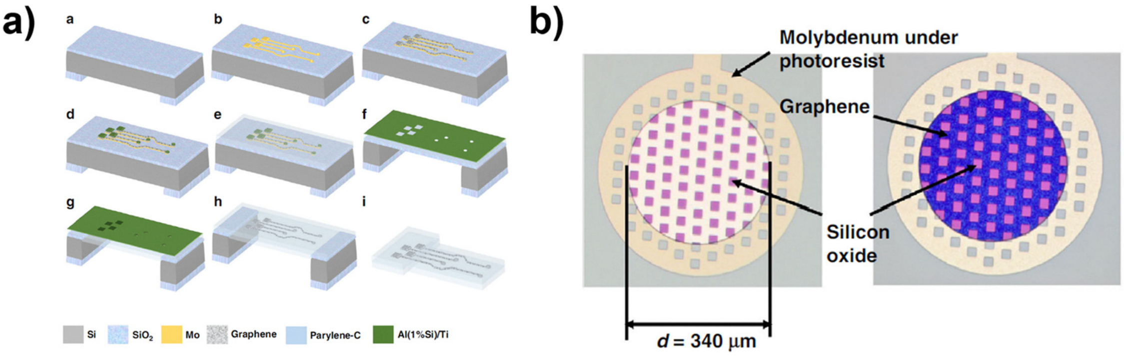

Fig. 8 Transfer-free fabrication process of molybdenum growth graphene electrodes (a). Close-up illustration of the prepared electrodes that showing the perforated structure of molybdenum and the resulting graphene electrode structure (b). Reproduced from ref. 31, with permission from Springer Nature, Copyright 2022.

In a recent study, Ramezani *et al.* employed a combination of double-layered graphene (DLG), chemical doping, and high-density NP deposition to fabricate the smallest (20 μm diameter) and the lowest per unit area impedance (0.78 Ω cm^2) transparent neural electrode interface to date.[55] The researchers followed the strategy of using the optical transmittance of the entire array except the PtNP deposited electrode regions (0.23%), and substituted the gold wires on the field of view with graphene wires. In order to avoid open circuits due to pinhole defects on thin graphene wires and reduce the high sheet resistance of single layer graphene (SLG) (1908 Ω sq^{-1}), researchers stacked two SLG graphene layers while immersing the first layer in HNO_3 solution for charge carrier doping of the interlayer. With this procedure the obtained interlayer doped double layer graphene (id-DLG) exhibited a sheet resistance of only 276 Ω sq^{-1}. The optical and electrochemical characterizations revealed the complete surface coverage of electrode regions by PtNP deposition increased the CSC by a factor of

7.5 and suppressed quantum capacitance effect of graphene electrodes.

It is also worth noting the development of CVD graphene coating on metal electrodes for neural electrode applications.[32,48,49] The use of graphene as a coating material in electrophysiological applications results in the loss of optical advantages of graphene but minimizes the risk of dead channel formation and offers superior long-term stability and biocompatibility as compared to its uncoated metal counterparts.

In two separate studies, Körbitzer *et al.* compared graphene, gold, and graphene-coated gold electrodes.[48,49] In the latter study, the group made use of microelectrodes for the purpose of measuring the impedances of the three types of electrodes at 1 kHz frequency.[48] The resulting electrode impedances were measured as 2.65 ± 0.26 MΩ, 1.08 ± 0.46 MΩ, and with a notable reduction on the graphene-coated gold electrode to 860 ± 70 kΩ, respectively. Impedance measurements were conducted on the electrodes following a period of four to six weeks of a full cell cultivation process and subsequent cleaning procedure. The objective of this study was to assess the stability of the electrodes under operational conditions. The findings revealed impedance increases of 34% for the gold electrodes, 2% for the graphene-coated gold electrodes, and no significant change in the impedance of the pure graphene. The reduced impedance levels are further reflected in the enhanced electrode capabilities, as CIC values of 0.16 ± 0.04 mC cm^{-2} and 0.15 ± 0.05 mC cm^{-2} were measured for gold and plain graphene, compared to 0.31 ± 0.02 mC cm^{-2} for graphene-coated gold electrodes. The neural recordings of electrodes show improved SNR levels of signals from 35.8 for gold electrodes to 66.6 for graphene-coated gold electrodes.

In the same year, a study by Park *et al.* investigated the effects of graphene coating on platinum.[32] Using circular and fractal electrodes of equal surface area, the researchers investigated the effect of coating on the dissolution problem of platinum electrodes, which is known to impair electrode performance and further induce toxic effects on neural cells. In the measurements, the uncoated fractal electrodes were found to have a CIC almost 3 times higher than the uncoated circular electrodes, while this value decreased by almost half after 10 hours of stimulation and exhibited a dissolution rate that was four-fold of the circular electrodes. The graphene coating of these fractal electrodes was observed to maintain the initial CIC values of these electrodes, while reducing Pt dissolution by 97% and showed limited performance decline in the CSC$_c$ and CIC measurements after 10 hours of continuous stimulation.

The neural electrodes referenced in the aforementioned studies were designed to be optimized through a range of surface modifications, fabrication techniques, and device design strategies through the incorporation of CVD graphene at varying layer counts. In evaluating these studies, which focus primarily on improving compatibility with optical methods and enhancing electrochemical conductivity, it is also important to consider the potential effects of these applications on the versatility, electrochemical stability, as well as the reduction in the elasticity of CVD graphene electrodes.

3.2. Graphene related material based neural electrodes

CVD graphene electrodes in solution exhibit exceptional stability and optical transparency, but their low ESA/GSA ratio, which limits the capacity for electrical double layer-based charge transfer, results in high electrochemical impedance for such electrodes. As a result, remote stimulation capability is limited compared to conductive polymer and nanostructured metal electrodes.[61–67] GRMs are widely adopted in neural electrode studies either in their bare form, with binders, or as fibers owing to their ability to diffuse electrolyte in stacked state, abundant functional groups, low fabrication cost, and intrinsic electrical and mechanical properties. In this regard, the implementation of GRM-based materials is of particular importance for *in vivo* and *in vitro* electrodes operating on thick neural tissue, as such materials can facilitate the separation of weak signals of far neurons or local field potentials from the electronic noise of the electrodes, as well as provide the ability to deliver effective stimulation to these dense networks.

The study by Chiu *et al.* is notable for being one of the first to investigate the use of GRMs for neural electrodes.[68] The researchers performed the biointeraction assay on a single isolated graphene sheet, thereby eliminating the effects of variations in stack thickness and packing density between studies of GRM electrodes. Silver paste was used to transfer the graphene flake onto a 300 μm diameter stainless steel needle electrode, and the relative change in the electrochemical properties compared to the uncoated control was studied by comparing changes in the charge transfer characteristics of electrodes implanted in the nervous system of American cockroach for up to 48 hours. The interpretation of the raw electrochemical measurements and the derived equivalent circuits indicated that the encapsulation effect induced by the immune response was significantly reduced in GNP-coated samples, providing evidence of improvement in biocompatibility.

Niaraki *et al.* performed electrohydrodynamic inkjet deposition of BSA-graphene solution to prepare neural electrodes from ball-milled GNP powder.[69] PI substrate surface was hydrophilized by polyethyleneimine (PEI) and polystyrene sulfonate (PSS) treatments prior to deposition. A vinyl mask was then employed in order to boost the patterning resolution of the water-based graphene inks to enable the fabrication of 200 μm wide linear electrode traces through a relatively wide 300 μm inkjet needle. Subsequently the electrodes were formed by heat treatment at 280 °C for 30 minutes in a convection oven. The research revealed no significant difference in the cytotoxicity levels as compared to the control group. An impedimetric cell sensor was developed based on the high cell binding capacity provided by the 3D micro-structured nature of the GNP ink fabricated electrodes. Experimental results demonstrated that the fabricated electrodes are able to accurately measure cell detachments in real time with a delay of less than 1 minute.

Unless GO materials are incorporated with an additional conductive material, rGO is often favored by researchers for GRM-based electrodes as its conductivity is several orders of magnitude higher than the GO precursors. In a study Murphy *et al.* presented a method for the scalable and efficient

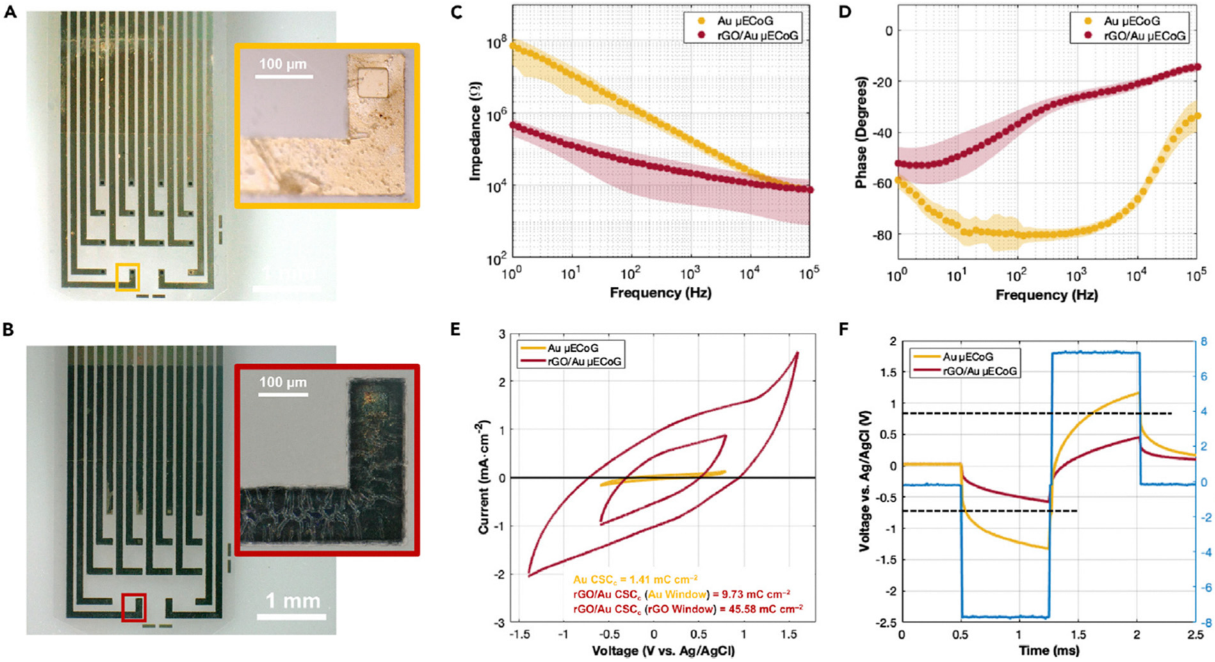

Fig. 9 Optical microscopy images of (A) bare Au and (B) rGO-coated microelectrodes with 50 × 50 μm contact openings. EIS (C) and (D), CV (E) and voltage transient measurements (F) of bare Au and rGO-coated electrodes. Reproduced from ref. 44 with permission from Elsevier, Copyright 2022.

production of high-performance rGO-based GRM coatings[44] (Fig. 9 and Table 2). Using a commercially available airbrush, the researchers sprayed a mixture of GO and the biocompatible reducing agent L-ascorbic acid (vitamin C) onto air plasma-treated Au–parylene C target surfaces. The sacrificial polymer layer around the pre-patterned gold regions was then manually removed from the surface, and the rGO-coated electrodes were finalized by vitamin C-assisted thermal reduction on a hot plate at 150 °C for 15 min, followed by patterning of the electrode regions (50 × 50 μm) *via* 4 um parylene C insulation. Despite the relatively low temperature reduction, spray-coated rGO films exhibited a comparable in-plane DC conductivity of 43 ± 4 S cm^{-1} for the films with a thickness of only 236 ± 26 nm. Regarding electrochemical performance, the wrinkled and multilayered rGO sheets of the GNP coating was found to reduce the 1 kHz impedance of bare gold electrodes from 177 ± 8 kΩ to 21 ± 18 kΩ. Concurrently, the CIC value of these electrodes increased from 0.36 mC cm^{-2} to 1.09 mC cm^{-2}. The rigorous endurance tests conducted with 500 μC cm^{-2} biphasic signals for 11 million cycles revealed that in contrast to the approximately 5-fold increased impedance rising in gold electrodes, there was no significant change in the impedance of the rGO-coated samples, indicating a substantially improved long-term stability for these electrodes.

Electrodeposition is a robust and widely adopted method for coating conductive substrates in a variety of applications as it allows a controlled and repeatable deposition under optimized parameters.[70–72] In 2019, Xiao *et al.* coated PtNP–rGO nanocomposites onto implantable metal microelectrode arrays with an electrode diameter of 25 μm.[73] The electrodeposition of composite was performed by application of −1 V for 50 s to electrodes in a mixed electrolyte consisting of chloroplatinic acid, lead acetate, and GO solution. Following deposition, the reduction of GO particles to rGO was achieved electrochemically by successive CV scans performed in PBS solution. Owing to the simultaneous deposition of both materials, the PtNP distribution on the layered and wrinkled GRM structure is further improved by the homogenization of nano materials and the resulting composite is reported to exhibit an 80-fold reduction in 1 kHz impedance compared to the bare Pt electrode.

Zhang *et al.* developed a novel one-step approach to prepare covalently functionalized amphiphilic rGO electrodes by compositing graphene oxide and insulating A-mPEG (hexamethylene diisocyanate-activated methoxypoly(ethylene glycol)) polymer with a cooccurring thermal reduction of GO.[74] As compared to the hydrazine-reduced rGO control sample, the mPEG functionalization was found to increase the colloidal stability and the composite is observed to remain stable for weeks. Furthermore the obtained mPEG–rGO composite showed a significant improvement of current response during CV measurements. The observed increase was attributed to the enhanced wettability of the electrodes. Subsequent experiments with PC12 cells revealed that the bioactivity of the PEG additive have enhanced the cell adhesion compared to the polystyrene-based tissue plate control and furthermore the composition with PEG also showed an improved electrical stimulation response ($\Delta F/F$) of the cells compared to chemically reduced rGO coated samples.

Increasing the thickness of thin films in flexible electrodes has been shown to improve electrochemical performance, but this improvement is often paralleled by an increased risk of film damage and fragmentation during bending operations.

Table 2 Summary of electrochemical characterizations reported in GRM studies

Material and method	Impedance @ 1 kHz	CSC	CIC	SNR	Electrode size	Notes	Ref.
rGO, air brush coating	21 ± 18 kΩ	1.41 mC cm^{-2} (200 mV s^{-1})^{a}	1.09 mC cm^{-2}	—	(50 × 50 μm)	*In vitro* dopamine sensor and *in vivo* neural Electrode tests included	44
Gold	177 ± 8 kΩ	9.73 mC cm^{-2} (200 mV s^{-1})^{ab}	0.36 mC cm^{-2}	—	(50 × 50 μm)		
PtNP–rGO composite, coating *via* e. deposition	32.75 kΩ	—	—	—	∅ 25 μm	Simultaneous dopamine concentration and neural spike sensor tests *in vivo* included	73
Uncoated Pt electrode	2.63 MΩ	—	—	—	∅ 25 μm		
rGO, compressed film transfer coating	25.2 ± 0.7 kΩ	45.9 mC cm^{-2} (100 mV)^{a}	∼4 mC cm^{-2}	—	∅ 25 μm	Extensive mechanical characterizations	75
LIG, CO$_2$ laser on PI	637 Ω	—	2 mC cm^{-2}	—	(250 × 250 μm)	*In vivo* tests included	34
HNO$_3$ doped LIG, CO$_2$ laser on PI	519 Ω	50 mC cm^{-2} (100 mV s^{-1})^{a}	3.1 mC cm^{-2}	—	(250 × 250 μm)		
LIG, CO$_2$ laser on PI	1.55 kΩ		3.2 mC cm^{-2}	—	(600 × 600 μm)	*Ex vivo* tests included	76
F doped LIG, CO$_2$ laser on fPI	—	362 mC cm^{-2} (100 mV s^{-1})	10.32 mC cm^{-2}	—	(600 × 600 μm)		
rGO fiber with 3D expanded tip, wet spin	—	50 mC cm^{-2} (100 mV s^{-1})^{a}	46 mC cm^{-2c}	—	102 000 μm^{2d}	*In vivo* and *in vitro* tests included	77
rGO fiber section, ∅ 25 μm, wet spin	8.7 MΩ (per μm^2)	798 mC cm^{-2} (100 mV s^{-1})	8.9 mC cm^{-2}	—	169 ± 25 μm^2	*In vivo* tests included	45
rGO fiber section, ∅ 25 μm with Pt collector	1.9 MΩ (per μm^2)	946 mC cm^{-2} (100 mV s^{-1})	10.5 mC cm^{-2}	—	169 ± 25 μm^2		
rGO fiber section, ∅ 40 μm	28.4 MΩ (per μm^2)	200 mC cm^{-2} (100 mV s^{-1})	4.7 mC cm^{-2}	—	749 ± 93 μm^2		
rGO fiber section, ∅ 40 μm with Pt collector	3.9 MΩ (per μm^2)	361 mC cm^{-2} (100 mV s^{-1})	8.0 mC cm^{-2}	9.2	749 ± 93 μm^2		
rGO fiber rod, wet spin	5768 Ω	7.97 mC cm^{-2} (100 mV s^{-1})	—	—	6.2 mm^2	*In vivo* tests included	78
rGO fiber rod 10% PEDOT:PSS	—	—	—	—	5.1 mm^2		
rGO fiber rod 20% PEDOT:PSS	3435 Ω	504 mC cm^{-2} (100 mV s^{-1})	—	—	4.7 mm^2		
rGO fiber rod 30% PEDOT:PSS	—	—	—	—	3.7 mm^2		
PPy GO (0.5 g L^{-1}) composite, electrodeposition	40 kΩ	242.17 mC cm^{-2} (50 mV s^{-1})^{e}	—	—	∅ 50 μm		79
PPy GO (1.0 g L^{-1}) composite, electrodeposition	26 kΩ	278.83 mC cm^{-2} (50 mV s^{-1})^{e}	—	—	∅ 50 μm		
PPy, electrodeposition	115 kΩ	190.98 mC cm^{-2} (50 mV s^{-1})^{e}	—	—	∅ 50 μm		
Bare Pt electrode	319 kΩ	0.94 mC cm^{-2} (50 mV s^{-1})^{e}	—	—	∅ 50 μm		
PEDOT-GO composite, electrodepositions	∼997 ± 52 Ω	∼ 86 ± 7.4 mC cm^{-2} (50 mV s^{-1})	∼4.71± 0.18 mC cm^{-2}	—	∅ 100 μm	*In vitro* biocompability tests included	43
Gold	20.59 kΩ	8.2 mC cm^{-2} (50 mV s^{-1})	0.16 mC cm^{-2}	—	∅ 100 μm		
PEDOT:PSS-GO(15) composite, electrodeposition	1.24 Ω (per cm^2)	82.75 mC cm^{-2} (50 mV s^{-1})	∼0.4 mC cm^{-2}		∅ 100 μm	*In vivo* tests included	33
PEDOT:PSS-rGO(15) composite, electrodeposition	0.59 Ω (per cm^2)	155.36 mC cm^{-2} (50 mV s^{-1})	∼7.0 mC cm^{-2}		∅ 100 μm		
Gold	∼2.5 Ω (per cm^2)	1.44 mC cm^{-2} (50 mV s^{-1})	∼0.1 mC cm^{-2}		∅ 100 μm		

[a] Cathodic CSC. [b] Calculated using the narrow Au potential window. [c] Theoretical calculation. [d] When the brush modelled as a disc. [e] Charge capacity density.

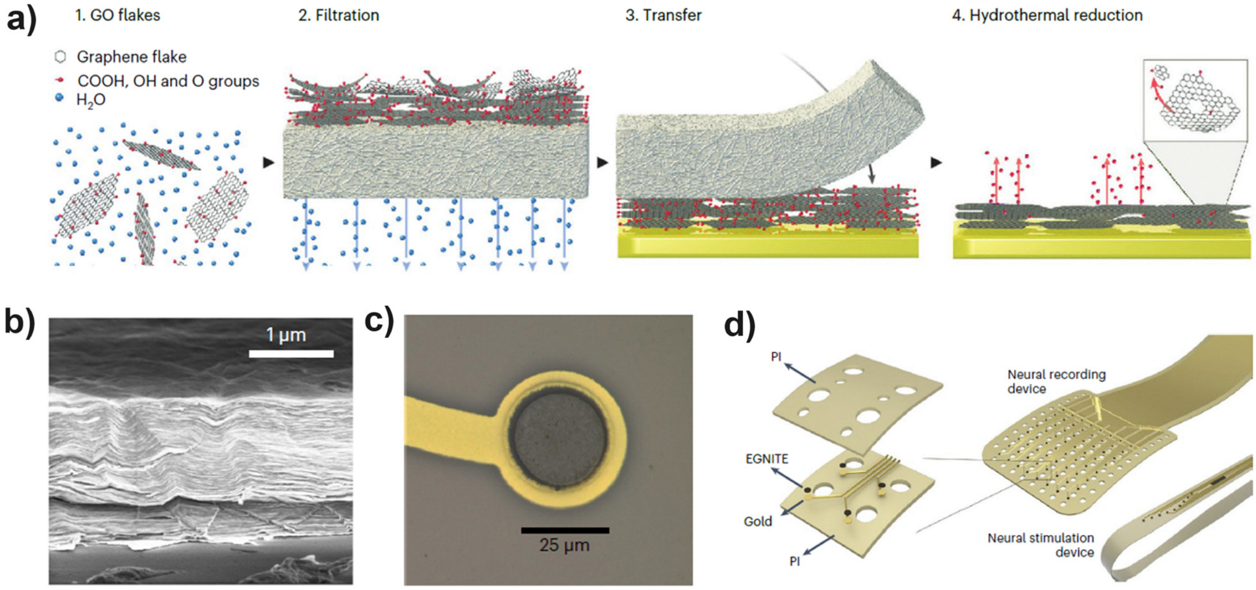

Fig. 10 Preparation and transfer of rGO thin films *via* EGNITE process (a). SEM image of the film cross-section showing dense package of rGO flakes (b). Optical image of the finalized rGO coating (c) and illustration of the final *in vivo* devices (d). Reproduced from ref. 75, with permission from Nature, Copyright 2024.

In their landmark study published in 2024, Viana and colleagues introduced a novel method for fabricating microelectrode array (MEA) through the Engineered Graphene for Neural Interface (EGNITE) process to overcome this limitation of GRM-based electrodes[75] (Fig. 10). During fabrication, the researchers initially processed an aqueous GO solution into a free-standing film through vacuum filtration process. The film was then transferred to PI substrate with pre-patterned gold connectors. Following this step the GO film was patterned by etching everywhere apart from the gold microelectrodes using oxygen reactive ion etching (RIE). Upon hydrothermal reduction of the transferred film, the rGO coatings were obtained with a thickness of 1 μm and an RMS roughness of 50 nm. In the later stages of fabrication, PI insulating layers were deposited to give the final form of the flexible MEA. The obtained flexible microelectrode arrays of EGNITE were thoroughly characterized in terms of physical, electrochemical and biological aspects. Despite its relatively thin structure, the electrode has demonstrated superior electrochemical performance, such as 25.2 ± 0.7 kΩ for the 1 kHz electrochemical impedance and a charge injection capacity of 4 mC cm^{-2} under 1 ms biphasic signals. Furthermore, an endurance test involving 15 million biphasic pulses resulted in no significant changes in impedance level and structural integrity, indicating a remarkably long electrochemical life of the electrodes. The electrodes are also mechanically tested in a demanding 37 kHz, 300 W ultrasonic stress test without cracking or delamination. A challenging bending test procedure around a 0.7 mm diameter rod was also performed and resulted in negligible impact on the EGNITE electrode impedance. In clinical studies, intracortical recordings of EGNITE from rat primary auditory cortex provided signals with SNR values greater than 30 dB. Long-term *in vivo* assays further revealed the ability of EGNITE to identify individual action potentials of nearby neurons for up to 1 month after implantation.

Laser-induced graphene (LIG) is a promising bottom-up fabrication method which can produce GRM in a rapid and scalable manner *via* selective pyrolysis of carbonaceous precursors. LIG has attracted considerable interest in a wide variety of research fields since its discovery in 2014, due to its ease of fabrication, low cost, and the significantly increased surface area of its highly porous 3D microstructure.[80–82] In addition to eliminating the need for traditional photolithographic patterning, the laser growth process effectively integrates the electrode with the substrate. In this way the LIG method also offers a new approach to ongoing efforts towards the adhesion stability of GRM's and flexible MEA's.

Using a 130 μm spot size CO_2 laser on a 50 μm thick flexible PI substrate, Lu *et al.* successfully created a uniform ECoG electrode array with edge lengths of 250 μm (Fig. 11, top).[83] By noting the LIG resolution can be reduced to 50 μm with the help of a simple shadow mask, the researchers continued fabrication by forming gold interconnects through photolithography and e-beam evaporation processes, and then MEA devices were obtained by spin-coating the surface with SU-8 encapsulation layer. The LIG electrodes prepared with an additional doping *via* 70% nitric acid treatment reported to lower the electrode impedance and increased the CIC of the LIG electrodes from 2 mC cm^{-2} to 3.1 mC cm^{-2}. The endurance test performed with 1 million cycles of biphasic stimulation reportedly did not lead to physical degradation of the LIG electrodes, however an overall increase in impedance values was noted in the EIS measurements. In addition, published data shows a significant variation between the impedance curves of the used

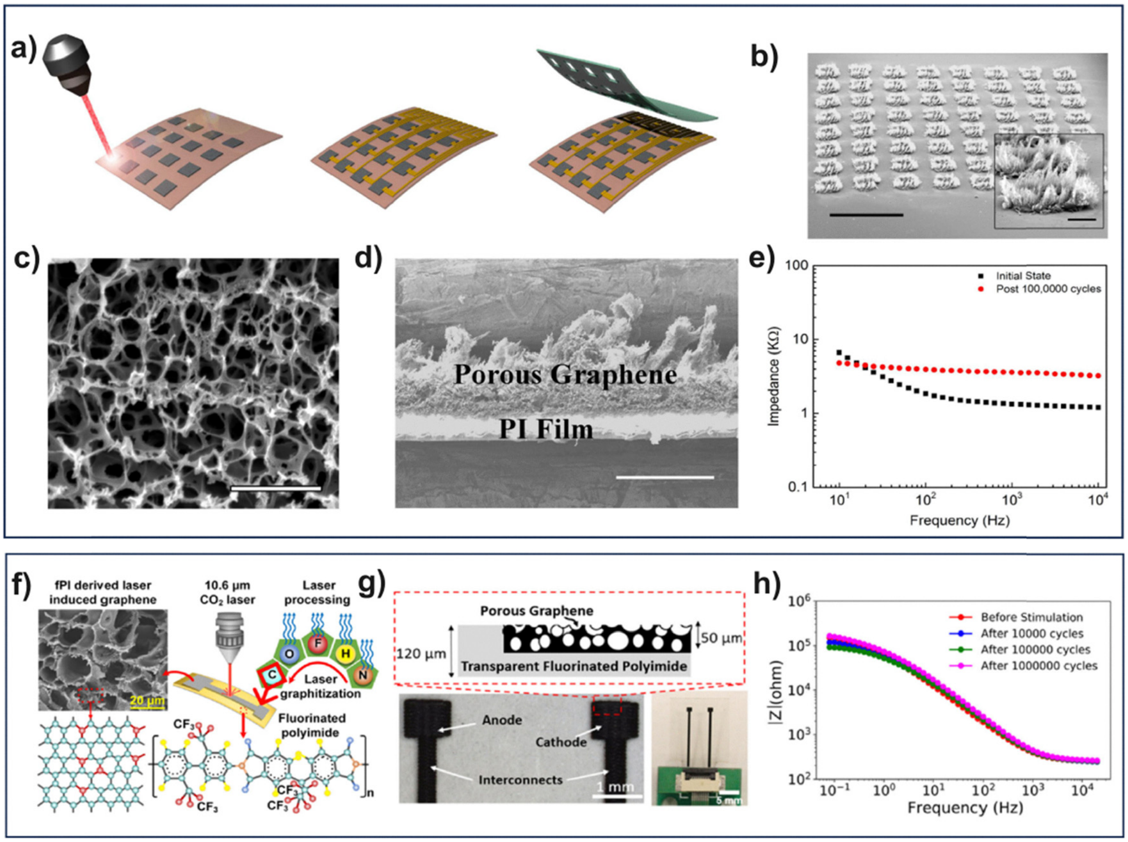

Fig. 11 Fabrication process of porous graphene electrode (a). SEM images of the porous graphene array showing the perforated and rough structure of LIG (b)–(d). The Altered profile of EIS spectrum after 100 000 cycles of biphasic stimulation pulses (e). Reproduced from ref. 83 with permission from Nature, Copyright 2016. Preparation of F-doped laser-induced graphene electrodes (fPI-3DPG) from fluorine incorporated polyimide precursor (f) and (g) and the stable EIS spectrum of fPI-3DPG even after 1 million pulse stimulation cycle (h). Reproduced from ref. 76 with permission from American Chemical Society, Copyright 2024.

and unused samples, which may indicate a variation in the charge transfer characteristics of the electrodes (Fig. 11e).

In 2024, Movaghgharnezhad *et al.* adopted an alternative approach to fabricate doped LIG neural electrodes by pretreating substrates with fluorine (Fig. 11, bottom).[76] To this end, the researchers prepared thin films from pure and fluorine-doped PI (fPI-3DPG and PI-3DPG) primers with a thickness of 120 μm and subsequently form minimeter-sized, 50-μm thick LIG electrode samples using a commercially available CO_2 laser engraving system. Results revealed that the fluorinated precursor-derived fPI-3DPG sample demonstrated a twofold increase in CIC compared to PI-3DPG and achieved significantly high capacity of 10.32 mC cm^{-2} at 1 ms pulse width. The authors attributed the increased CIC of fPI-3DPG to the formation of gaseous by-products during the pyrolysis of the fluorinated precursor, which induced the formation of intense micro/nano-porosity and significantly increased the specific surface area of the electrodes. This physical modification explanation for the increased CIC is further supported by the strong capacitive behavior observed in the EIS spectrum of the fPI-3DPG sample (Fig. 10h). Despite the relatively high GRM thickness (50 μm), the fPI-3DPG electrodes were maintained stable electrochemical performance after a series of tests, including 10 000 bending cycles at 4.5% bending strain, 1000 consecutive CV scans, and application of 1 million biphasic pulse stimulations. Remarkably, unlike the previous LIG study by Lu *et al.* in 2016,[83] the fPI-3DPG electrodes exhibited an unchanged EIS profile even after 1 million stimulations. Although these improvements of fPI-3DPG electrodes are promising for LIG studies, it would be worthwhile to first investigate whether the remarkable resistance to bending damage of such wide and thick LIGs can be replicated in micro-scale electrode arrays.

As a distinct innovation from the planar GRM electrode arrays, GRM-based free-standing microelectrodes offer a viable alternative to existing metal and silicon-based penetrating electrodes used *in vivo* applications due to advantages such as the biologically relevant flexible and low-density structure, high mechano-environmental stability, as well as the superior electrochemical performance that allow further miniaturization of the electrodes.[5,45,84]

In their widely recognized pioneering work, Apollo *et al.* used the wet spinning method to produce free-standing graphene fiber (GF) electrodes.[77] Reduced liquid crystal graphene oxide (LCGO) fibers with an elastic modulus of 11.2 GPa were obtained by forming a solution of LCGO and later processing

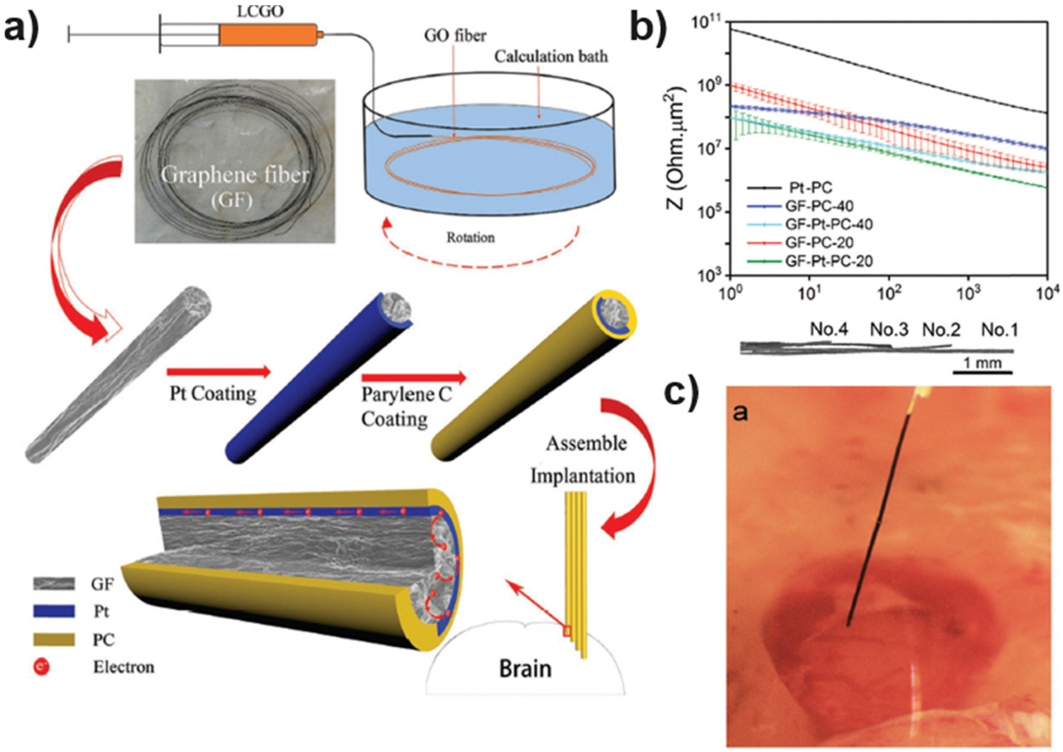

Fig. 12 Preparation steps of GF–Pt–Parylene C electrodes by wet spinning method and subsequent coating processes (a). The impedance spectrum of Pt control and prepared samples (b). Hand assembled MEA of fibers (top) and insertion of GF–Pt–Parylene C-40 sample for *in vivo* recording (c). Reproduced from ref. 45 with permission from John Wiley and Sons, copyright 2019.

the solution into fibers by $CaCl_2$ coagulation and finally reducing the fibers by vacuum annealing process. Subsequently, the obtained fibers were insulated with a Parylene C coating and then underwent laser cutting to remove the excess insulation at the extremity of the fibers. This process resulted in a ''brush-like'' expansion of the 3D electrode, making the exposed tips 3.5 times wider than the 50 μm thickness of the as-prepared fibers. The researchers theoretically calculated an extraordinarily high charge injection capacity (Q_{inj}) of 46 mC cm^{-2} based on the electrode GSA and the double layer capacitance of the EIS equivalent circuit and argued that laser ablation was the key to achieving it.

Wang *et al.* produced LCGO-based fibers with diameters ranging from 20 to 40 μm by a wet spinning process followed by *in situ* reduction in a coagulation bath containing hypophosphorous acid (Fig. 12).[45] Along with different fiber thicknesses, the effect of the conductive Pt coating on the 40 μm (dry conductivity 52 ± 0.3 S cm^{-1}) and 20 μm (dry conductivity 205 ± 16 S cm^{-1}) thick graphene fibers investigated. The application of a 200 nm thick Pt coating was reported to further increase the conductivity of fibers up to 460 ± 30 S cm^{-1}. Electrochemical characterization of GF, platinum-coated graphene fiber (GF–Pt), and platinum wire (Pt) control was performed after insulating the samples with 2 μm thick Parylene-C and opening a planar electrode site by dipping the probe tips into liquid nitrogen. The GF-20 sample was found to reduce the 1 kHz impedance of the 500 MΩ μm^{-2} platinum wire control by a factor of 50. In addition, the coatings of platinum collector of graphene fibers decreased the per area impedance observed on the GF-20 electrodes by approximately 5 times and the GF-40 electrodes by ∼10 times compared to their uncoated counterparts. Among the experimental measurements of the charge injection capacity, the highest CIC was obtained with the GF–Pt-20 sample as 10.5 mC cm^{-2}. The *in vivo* tests in rat cerebral cortex further demonstrated that platinum-coated GF–Pt electrodes can record single-unit waveforms with higher SNR than GF electrodes. Researchers attributed the superior per unit area performance of the thinner and platinum-coated electrodes to the higher electronic conductivity of the samples.

In 2022, Xiong *et al.* developed soft PEDOT:PSS-rGO fiber (PGF) composite electrodes as an alternative to conductive polymer coatings on rigid freestanding electrodes, which are prone to suffer from delamination due to poor substrate-coating interactions.[78] To form PEDOT composite fibers, researchers added 10, 20 and 30 wt% PEDOT into the GO spinning solutions and prepared the fibers by wet spinning. After the fibers were prepared, the GO content was reduced by hydroiodic acid treatments. Based on stress–strain tests, it was reported that the optimum mechanical properties were obtained with the PGF-20 sample, as it had the highest tensile strength (35 MPa) among the three samples. The CV measurements of the PGF-20 showed a CSC of 504 mC cm^{-2}, a value approximately 60 times higher than that of the GF control sample. The team also performed an electrochemical durability test on the PGF-20 composite sample by performing 1000 consecutive CV scans on the electrode and demonstrated an 80% retention of the original CSC.

The aforementioned studies provide evidence that the specific surface area, functional group density, and electrical conductivity of GRMs strike an important balance for the biocompatibility and electrochemical performance of neural electrodes. Moreover, the distinct fabrication processes were further explored in these works that produce substrate-attached and the *in vivo-optimized* free-standing electrodes that exhibit high mechanical durability while offering elasticity and providing a high electrochemical conductivity to produce effective tissue stimulations.

3.2.1. Conductive polymer–GRM composite neural electrodes. One of the major branches of GRM-based neural electrodes involves the incorporation of powder form GRMs with conducting polymers (CPs) such as PPy and PEDOT.[43,79,85,86] The formation of these composites contributes to the stability of the carbon based materials by preventing the dissolution of electrodes, while on the CP side an improvement in mechanical stability and electrochemical performance is widely observed as compared to their pristine forms.[43,79,86]

Deng *et al.* electrochemically deposited a PPy–GO composite onto the pre-patterned platinum neural electrodes for investigating the effect of deposition current density and GO concentration on electrode performance(Fig. 13).[79] SEM images of the study revealed that the effective surface area of the composites increased significantly with higher GO ratios and current densities through enhancing electrode surface roughness and outgrowth. Composite samples prepared with GO concentrations of 0.5 g L^{-1} and 1.0 g L^{-1} were further subjected to electrochemical characterizations, and improved responses were obtained with the increased GO content in the composite. Importantly, increasing the deposition charge density from 0.5 C cm^{-2} to 2 C cm^{-2} resulted in higher outgrowths for all GO composites, whereas the pristine PPy electrodes were found to be collapsed at the polymerization currents above 2 C cm^{-2}. The results show a 4-fold decrease for 1 kHz impedance and a 1.5-fold increase for CSC measurements with the best performing composite compared to the bare PPy electrode.

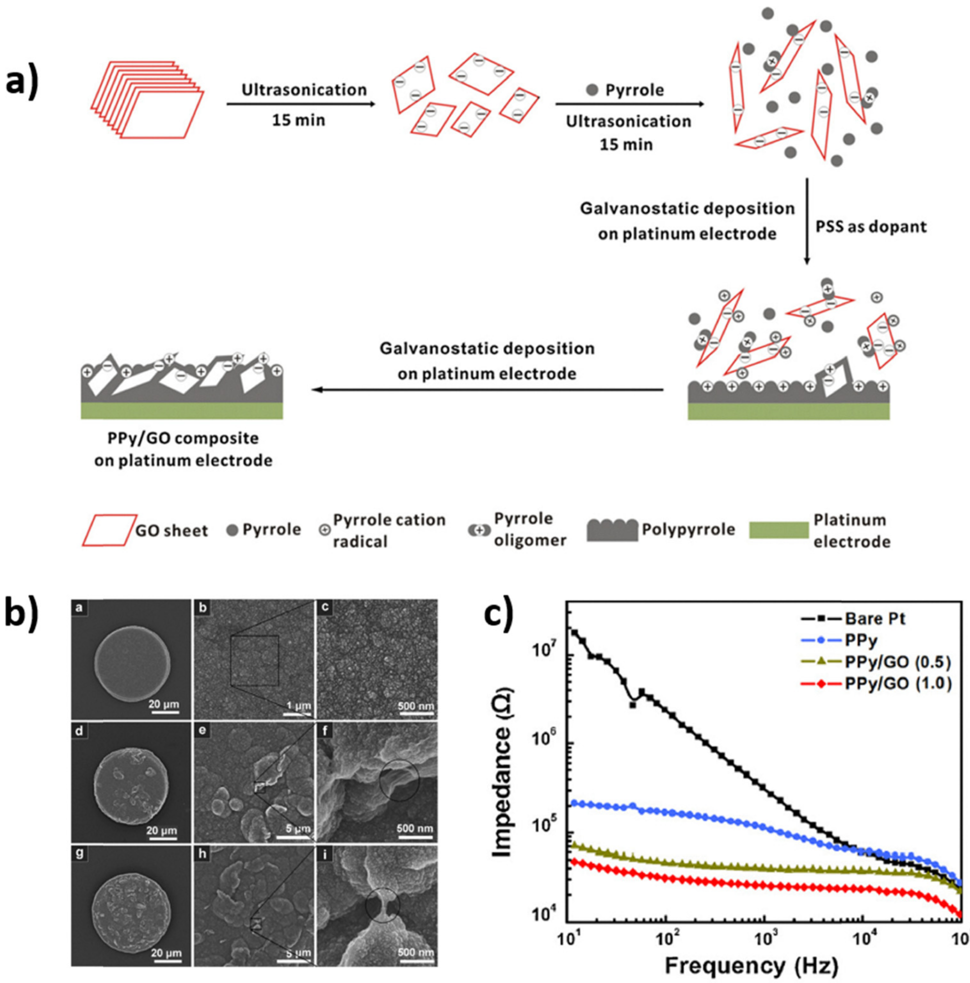

Fig. 13 Deposition process of PPy on electrode sites by ultrasonic exfoliation of GO–Pyrrole/PSS introduction and electrochemical application (a). SEM images of deposited films showing rough surface for composites (top PPy, middle PPy/GO 0.5, bottom PPy/GO1.0) (b). The lowered impedance of bare PPy and PPy/GO coated Pt electrodes (c). Reproduced from ref. 79 with permission from Elsevier, copyright 2011.

In a similar study, graphene oxide was incorporated into PEDOT polymer and electrodes have been studied in terms of their physical electrochemical and bio interactions.[43] The experimental set of the study consists of gold electrodes coated with a hybrid solution of 2 mg mL^{-1} GO and 0.01 M -EDOT at different deposition times ranging from 10 to 40 minutes. Measured CSC for bare gold electrodes was 8.27 mC cm^{-2} and for composite coatings averaged 86.74 mC cm^{-2}, with an increase proportional to the deposition time. The obtained CSC results and EIS data were interpreted in detail along with the derived EIS equivalent circuits of the samples. Stimulation tests performed at 1 ms pulse duration were reported to achieve an average CIC of 4.71 mC cm^{-2} with composite electrodes, a 30-fold increase compared to the gold electrode. Bioassays performed with the PC-12 cell line showed superior cell adhesion of the composite electrodes *versus* the gold electrodes, and the composites had no negative effect on neuronal proliferation as compared to the gold electrodes and cell plate. In this regard, the study highlighted that the cytotoxic activity of GO interactions may have been suppressed by the polymer encapsulation.

PSS are often used in combination with PEDOT (poly(3,4-ethylenedioxythiophene) to avoid mechanical problems such as swelling, shrinkage, and dissolution of the PEDOT electrode by stimulation applications and the medium itself.[87–89] Lee *et al.* thoroughly investigated the effect of varying oxidation levels of GO materials and the rGO materials obtained by reduction of these materials on the PEDOT:PSS based GRM composite electrodes.[86] The GO samples were prepared by oxidizing 0.1 g of graphite with 0.05 g (GO5), 0.15 g (GO15), and 0.25 g (GO25) of $KMnO_4$, and the reduced samples were derived from acid-aluminum assisted reduction of these starting materials. The GO and rGO materials were then dispersed with PEDOT:PSS polymers electrodeposited on gold electrodes, and finally characterized *via* EIS, CSC and CIC techniques. Samples with adequate oxidation (GO15 and GO25) were observed to have significantly improved electrochemical properties with the reductions and also had the best performance among all other specimens. Instead of rGO25, the optimal electrode performances were obtained with rGO15 composite, and this finding was explained by the reduced in-plane conductivity of the extensively oxidized and thus deformed structure of GO25 precursor. Nanoindentation measurements surprisingly reveal that GO and rGO doping in PEDOT:PSS reduces the modulus of electrodes from 7.3 GPa to 2–5 GPa, which is attributed to the formation of pores by the incorporation of GRM particles. Experiments carried out with PC12 cells showed that composites formed using both GO and rGO significantly increased the levels of the intercellular communication genes of GAP-43 and synapsin compared to control samples.

Besides oxidation and reduction, heteroatom doping on GRM is a modification method that has been evaluated by a number of electrochemical studies.[90–92] To investigate the effect of N-doping of the GRM in neural electrode applications, Fan *et al.* electrodeposited a mixture of 2 mg mL^{-1} GO and 0.01 M EDOT solution and then applied a post-reduction treatment to prepare N-rGO-doped PEDOT electrodes.[85] The researchers prepared and characterized microorganism reduced N-doped rGO (PEDOT-NrGO), hydrazine hydrate reduced N-doped rGO (PEDOT-HrGO), unreduced GO (PEDOT-GO), and a blank PEDOT electrode sample. Both EIS measurements and CV scans revealed an increase in the electrochemical conductivity and capacitive properties of the N-rGO sample as compared to blank PEDOT and PEDOT-GO samples. Cyclic voltammetry measurements were conducted on PEDOT and PEDOT/N-rGO electrodes over 200 cycles at a scan rate of 5 mV s^{-1}. The nearly unchanged cyclic voltammetry curves of PEDOT/N-rGO compared to pristine samples demonstrate that incorporating N-rGO significantly enhances the electrochemical stability of PEDOT electrodes. Previously, another article attributed this improvement to rGO flakes reinforcing the PEDOT matrix by holding together the polymer chains, that tend to fragment or exfoliate during electrochemically driven redox reactions.[43] Finally, the authors noted that the bioassisted reduction of GO (N-rGO) mitigated the decrease in cell viability commonly seen with GO and HrGO composites.

Furthermore the improvements achieved through GRM doping of conductive polymer-based neural electrodes open important opportunities for flexible string/net-based electrode designs, where these matrices are widely used.[93–96] Such composite electrodes can be readily fabricated *via* the same electrodeposition techniques used for pristine conducting polymers and present several important advantages, including reduced geometric dimensions, improved electrochemical conductivity, enhanced flexibility, and stable long-term performance.

4. Future challenges and outlook

Though the encouraging outcomes demonstrated by neural electrodes, whether graphene or GRM-based, there exist substantial drawbacks that hinder their transition to clinical implementation. The most significant challenges to be addressed include the long-term stability of electrodes, scalability and reproducibility, device integration, performance consistency, and potential neurotoxicity. Despite the enhancement of biocompatibility to an acceptable level, as evidenced by modifications documented in the literature, microglial/astrocyte activation and the subsequent glial scar/fibrous encapsulation persist as significant impediments to long-term performance. These alterations have been shown to increase impedance and distort signals, which can adversely affect outcomes. As demonstrated in the comprehensive review of the extant literature,[97] there is a clear need for further research in this field. Specifically, there is a small number of long-term stability studies that are conducted under physiological conditions (electrolytes, enzymes, mechanical stress) and electrical pulses. Moreover, the long-term *in vivo* data that is currently available appears to be insufficient. It is imperative that rigorous, long-term (months to years) studies are conducted in relevant animal models to evaluate the chronic biocompatibility, stability and functional performance of different graphene-based electrodes. Systematic studies employing fully characterized materials in accordance with emerging standards are required to precisely correlate specific material properties (size, layers, functionalization, purity, defects) with *in vivo* neurotoxicity results over extended periods of time. It is necessary to comprehend the nature of degradation products and their associated effects.[98,99]

There is a necessity for a more profound comprehension of the interactions between the surface properties of graphene and biological components, with particular emphasis on the interaction with immune system cells, such as microglia.[100] Such interactions include protein adsorption, cell adhesion mechanisms, and charge transfer physics. In addition, the specific roles of material properties, such as defects, functional groups, and topography, in eliciting biological responses, including inflammation, toxicity, and regeneration, must be elucidated.[101]

There is an inverse relationship between the scalability/cost-effectiveness of graphene production methods and the quality/repeatability of the resulting material. Methods suitable for batch production (*e.g.*, some exfoliation or GO/rGO routes) often yield materials with higher variability and defects compared to more controlled but less scalable methods (such as CVD). This trade-off poses a significant barrier to reliably and affordably produce medical-grade graphene.[102] The high cost of high-quality graphene production and complex fabrication processes can be a barrier compared to established technologies, and scalable, low-cost production is needed for clinical translation.[103]

In summary, beyond the technical challenges, graphene-based neural electrodes must overcome regulatory, standardization and cost barriers to successfully move from the laboratory to the clinic. As with all new implants, gaining approval for neural ones is a significant hurdle. The inherent variability and complexity of graphene materials has been identified as a significant factor contributing to the complexity of the already challenging regulatory approval process.

5. Conclusion

Neural electrodes serve as the central interfaces to facilitate bidirectional communication between biological entities and external electronics for basic research, disease treatment and neuroprosthetic applications. Electrochemically interacting neural electrodes are specialized interfaces that facilitate the precise and reliable transmission of neural signals, including low-amplitude single unit activities and local field potentials of neuron populations. These interfaces additionally allow for the effective and precise electrical manipulation of neurons and offer a sophisticated tool for neural engineering and research applications. The biocompatibility requirements for these invasive electrodes establish novel standards in terms of chemical and mechanical properties. In combination, the reduced dimensions of the electrodes allow for better tissue integration and greater application specificity but also introduce significant electrochemical challenges on the materials front. Depending on the preferred type of graphene, the graphene and graphene-related nanomaterials in the fabrication of micro-sized electrochemical neural electrodes are enabling the devices to offer increased electrochemical surface area, improved operational stability, enhanced biomechanical compatibility, superior mechanical durability, and optical transparency features. Current research efforts in the area focus primarily on innovative fabrication methods for graphene-based electrodes, along with the incorporation of chemical doping, nanoparticle deposition, and polymer composite modifications toward subcellular-scale electrodes. Future studies are expected to benefit from the insight, methodologies and modification routes of the existing literature and further promote the development of high-performing, robust and multifunctional graphene-based electrodes for research and clinical applications.

Conflicts of interest

There are no conflicts to declare.

Data availability

No primary research results, software or code have been included and no new data were generated or analysed as part of this review.

References

1 P. Johns, Overview of the nervous system, *Clinical Neuroscience*, Elsevier, 2014, pp. 1–17, DOI: 10.1016/B978-0-443-10321-6.00001-1.

2 C. R. Noback, N. L. Strominger, R. J. Demarest and D. A. Ruggiero, *Neurons and Associated Cells, The Human Nervous System*, Humana Press, Totowa, NJ, 2005, pp. 11–39, DOI: 10.1007/978-1-59259-730-7_2.

3 Q. Zeng, X. Li, S. Zhang, C. Deng and T. Wu, Think big, see small—A review of nanomaterials for neural interfaces, *Nano Select*, 2022, **3**, 903–918.

4 C. Boehler, S. Carli, L. Fadiga, T. Stieglitz and M. Asplund, Tutorial: guidelines for standardized performance tests for electrodes intended for neural interfaces and bioelectronics, *Nat. Protoc.*, 2020, **15**, 3557–3578.

5 S. F. Cogan, Neural Stimulation and Recording Electrodes, *Annu. Rev. Biomed. Eng.*, 2008, **10**, 275–309.

6 T. D. Y. Kozai, A. S. Jaquins-Gerstl, A. L. Vazquez, A. C. Michael and X. T. Cui, Brain Tissue Responses to Neural Implants Impact Signal Sensitivity and Intervention Strategies, *ACS Chem. Neurosci.*, 2015, **6**, 48–67.

7 S. F. Cogan, D. J. Garrett and R. A. Green, Electrochemical Principles of Safe Charge Injection, in *Neurobionics: The Biomedical Engineering of Neural Prostheses*, ed. R. K. Shepherd, Wiley, 2016, pp. 55–88, DOI: 10.1002/9781118816028.ch3.

8 C. Bedard, C. Piette, L. Venance and A. Destexhe, Extracellular and intracellular components of the impedance of neural tissue, *Biophys. J.*, 2022, **121**, 869–885.

9 J. Rivnay, H. Wang, L. Fenno, K. Deisseroth and G. G. Malliaras, Next-generation probes, particles, and proteins for neural interfacing, *Sci. Adv.*, 2017, **3**, e1601649.

10 C. Liang, *et al.*, Strategies for interface issues and challenges of neural electrodes, *Nanoscale*, 2022, **14**, 3346–3366.

11 M. Ferguson, D. Sharma, D. Ross and F. Zhao, A Critical Review of Microelectrode Arrays and Strategies for Improving Neural Interfaces, *Adv. Healthcare Mater.*, 2019, **8**, 1900558.

12 M. Zhang, Z. Tang, X. Liu and J. Van Der Spiegel, Electronic neural interfaces, *Nat. Electron.*, 2020, **3**, 191–200.

13 H. Yuk, B. Lu and X. Zhao, Hydrogel bioelectronics, *Chem. Soc. Rev.*, 2019, **48**, 1642–1667.

14 J. Scholvin, *et al.*, Close-Packed Silicon Microelectrodes for Scalable Spatially Oversampled Neural Recording, *IEEE Trans. Biomed. Eng.*, 2016, **63**, 120–130.

15 D. Kuzum, *et al.*, Transparent and flexible low noise graphene electrodes for simultaneous electrophysiology and neuroimaging, *Nat. Commun.*, 2014, **5**, 5259.

16 B. Xu, J. Pei, L. Feng and X.-D. Zhang, Graphene and graphene-related materials as brain electrodes, *J. Mater. Chem. B*, 2021, **9**, 9485–9496.

17 Y. Lu, X. Liu and D. Kuzum, Graphene-based neurotechnologies for advanced neural interfaces, *Curr. Opin. Biomed. Eng.*, 2018, **6**, 138–147.

18 N. A. Kotov, *et al.*, Nanomaterials for Neural Interfaces, *Adv. Mater.*, 2009, **21**, 3970–4004.

19 S. P. Lacour, G. Courtine and J. Guck, Materials and technologies for soft implantable neuroprostheses, *Nat. Rev. Mater.*, 2016, **1**, 16063.

20 Z. Suo, E. Y. Ma, H. Gleskova and S. Wagner, Mechanics of rollable and foldable film-on-foil electronics, *Appl. Phys. Lett.*, 1999, **74**, 1177–1179.

21 D.-W. Park, *et al.*, Graphene-based carbon-layered electrode array technology for neural imaging and optogenetic applications, *Nat. Commun.*, 2014, **5**, 5258.

22 Y. Lu, *et al.*, Ultralow Impedance Graphene Microelectrodes with High Optical Transparency for Simultaneous Deep Two-Photon Imaging in Transgenic Mice, *Adv. Funct. Mater.*, 2018, **28**, 1800002.

23 Y. U. Cho, S. L. Lim, J.-H. Hong and K. J. Yu, Transparent neural implantable devices: a comprehensive review of challenges and progress, *npj Flexible Electron.*, 2022, **6**, 53.

24 M. Thunemann, *et al.*, Deep 2-photon imaging and artifact-free optogenetics through transparent graphene microelectrode arrays, *Nat. Commun.*, 2018, **9**, 2035.

25 D.-W. Park, *et al.*, Electrical Neural Stimulation and Simultaneous *in Vivo* Monitoring with Transparent Graphene Electrode Arrays Implanted in GCaMP6f Mice, *ACS Nano*, 2018, **12**, 148–157.

26 A. R. Harris, *et al.*, Conducting polymer coated neural recording electrodes, *J. Neural Eng.*, 2013, **10**, 016004.

27 S. Yaeli, Form-function relations in cone-tipped stimulating microelectrodes, *Front. Neuroeng.*, 2009, **2**, 13.

28 G. Schiavone, *et al.*, Guidelines to Study and Develop Soft Electrode Systems for Neural Stimulation, *Neuron*, 2020, **108**, 238–258.

29 T. L. Rose and L. S. Robblee, Electrical stimulation with Pt electrodes. VIII. Electrochemically safe charge injection limits with 0.2 ms pulses (neuronal application), *IEEE Trans. Biomed. Eng.*, 1990, **37**, 1118–1120.

30 S. B. Brummer and M. J. Turner, Electrochemical Considerations for Safe Electrical Stimulation of the Nervous System with Platinum Electrodes, *IEEE Trans. Biomed. Eng.*, 1977, **BME-24**, 59–63.

31 N. Bakhshaee Babaroud, *et al.*, Multilayer CVD graphene electrodes using a transfer-free process for the next generation of optically transparent and MRI-compatible neural interfaces, *Microsyst. Nanoeng.*, 2022, **8**, 107.

32 H. Park, S. Zhang, A. Steinman, Z. Chen and H. Lee, Graphene prevents neurostimulation-induced platinum dissolution in fractal microelectrodes, *2D Mater.*, 2019, **6**, 035037.

33 S. Lee, T. Eom, M.-K. Kim, S.-G. Yang and B. S. Shim, Durable soft neural micro-electrode coating by an electrochemical synthesis of PEDOT:PSS/graphene oxide composites, *Electrochim. Acta*, 2019, **313**, 79–90.

34 Y. Lu, H. Lyu, A. G. Richardson, T. H. Lucas and D. Kuzum, Flexible Neural Electrode Array Based-on Porous Graphene for Cortical Microstimulation and Sensing, *Sci. Rep.*, 2016, **6**, 33526.

35 T. A. M. Suter, *et al.*, Engineering Catalyst Layers for Next-Generation Polymer Electrolyte Fuel Cells: A Review of Design, Materials, and Methods, *Adv. Energy Mater.*, 2021, **11**, 2101025.

36 T. S. Mathis, *et al.*, Energy Storage Data Reporting in Perspective—Guidelines for Interpreting the Performance of Electrochemical Energy Storage Systems, *Adv. Energy Mater.*, 2019, **9**, 1902007.

37 E. K. Brunton, *et al.*, In vivo comparison of the charge densities required to evoke motor responses using novel annular penetrating microelectrodes, *Front. Neurosci.*, 2015, **9**, 265.

38 A. C. Lazanas and M. I. Prodromidis, Electrochemical Impedance Spectroscopy—A Tutorial, *ACS Meas. Sci. Au*, 2023, **3**, 162–193.

39 S. B. Hladky and M. A. Barrand, Mechanisms of fluid movement into, through and out of the brain: evaluation of the evidence, *Fluids Barriers CNS*, 2014, **11**, 26.

40 S. B. Baumann, D. R. Wozny, S. K. Kelly and F. M. Meno, The electrical conductivity of human cerebrospinal fluid at body temperature, *IEEE Trans. Biomed. Eng.*, 1997, **44**, 220–223.

41 P. Takmakov, *et al.*, Rapid evaluation of the durability of cortical neural implants using accelerated aging with reactive oxygen species, *J. Neural Eng.*, 2015, **12**, 026003.

42 D. W. L. Hukins, A. Mahomed and S. N. Kukureka, Accelerated aging for testing polymeric biomaterials and medical devices, *Med. Eng. Phys.*, 2008, **30**, 1270–1274.

43 H.-C. Tian, *et al.*, Graphene oxide doped conducting polymer nanocomposite film for electrode-tissue interface, *Biomaterials*, 2014, **35**, 2120–2129.

44 B. B. Murphy, *et al.*, Vitamin C-reduced graphene oxide improves the performance and stability of multimodal neural microelectrodes, *iScience*, 2022, **25**, 104652.

45 K. Wang, *et al.*, High-Performance Graphene-Fiber-Based Neural Recording Microelectrodes, *Adv. Mater.*, 2019, **31**, 1805867.

46 W. Franks, I. Schenker, P. Schmutz and A. Hierlemann, Impedance Characterization and Modeling of Electrodes for Biomedical Applications, *IEEE Trans. Biomed. Eng.*, 2005, **52**, 1295–1302.

47 B. Halliwell, Reactive Oxygen Species and the Central Nervous System, *J. Neurochem.*, 1992, **59**, 1609–1623.

48 B. Körbitzer, P. Krauß, S. Belle, J. J. Schneider and C. Thielemann, Electrochemical Characterization of Graphene Microelectrodes for Biological Applications, *ChemNanoMat*, 2019, **5**, 427–435.

49 B. Koerbitzer, *et al.*, Graphene electrodes for stimulation of neuronal cells, *2D Mater.*, 2016, **3**, 024004.

50 D. Nguyen, *et al.*, Novel graphene electrode for retinal implants: an in vivo biocompatibility study, *Front. Neurosci.*, 2021, **15**, 615256.

51 A. El Merhie, *et al.*, Single layer graphene functionalized MEA for enhanced detection of neuronal network development, *Sens. Actuators, B*, 2018, **277**, 224–233.

52 S. K. Krishnan, N. Nataraj, M. Meyyappan and U. Pal, Graphene-Based Field-Effect Transistors in Biosensing and Neural Interfacing Applications: Recent Advances and Prospects, *Anal. Chem.*, 2023, **95**, 2590–2622.

53 D. Kireev, *et al.*, Graphene Multielectrode Arrays as a Versatile Tool for Extracellular Measurements, *Adv. Healthcare Mater.*, 2017, **6**, 1601433.

54 A. Bourrier, *et al.*, Monolayer Graphene Coating of Intracortical Probes for Long-Lasting Neural Activity Monitoring, *Adv. Healthcare Mater.*, 2019, **8**, 1801331.

55 M. Ramezani, *et al.*, High-density transparent graphene arrays for predicting cellular calcium activity at depth from surface potential recordings, *Nat. Nanotechnol.*, 2024, **19**, 504–513.

56 Y. Wang, *et al.*, Electrochemical Delamination of CVD-Grown Graphene Film: Toward the Recyclable Use of Copper Catalyst, *ACS Nano*, 2011, **5**, 9927–9933.

57 T. Fang, A. Konar, H. Xing and D. Jena, Carrier statistics and quantum capacitance of graphene sheets and ribbons, *Appl. Phys. Lett.*, 2007, **91**, 092109.

58 L. D'Arsié, *et al.*, Stable, efficient p-type doping of graphene by nitric acid, *RSC Adv.*, 2016, **6**, 113185–113192.

59 S. Tahmasebi, *et al.*, How Stable Are Spherical Platinum Nanoparticles Applied to Fuel Cells?, *J. Phys. Chem. C*, 2018, **122**, 11765–11776.

60 D.-W. Park, *et al.*, Fabrication and utility of a transparent graphene neural electrode array for electrophysiology, in vivo imaging, and optogenetics, *Nat. Protoc.*, 2016, **11**, 2201–2222.

61 T. Sun, *et al.*, Flexible IrOx neural electrode for mouse vagus nerve stimulation, *Acta Biomater.*, 2023, **159**, 394–409.

62 Y. H. Kim, *et al.*, *In vitro* extracellular recording and stimulation performance of nanoporous gold-modified multi-electrode arrays, *J. Neural Eng.*, 2015, **12**, 066029.

63 M. Leber, *et al.*, Long term performance of porous platinum coated neural electrodes, *Biomed. Microdevices*, 2017, **19**, 62.

64 C. Boehler, T. Stieglitz and M. Asplund, Nanostructured platinum grass enables superior impedance reduction for neural microelectrodes, *Biomaterials*, 2015, **67**, 346–353.

65 S. Venkatraman, *et al.*, PEDOT coated microelectrode arrays for chronic neural recording and stimulation. in 2009 4th International IEEE/EMBS Conference on Neural Engineering 383–386 (IEEE, Antalya, Turkey, 2009), DOI: 10.1109/NER.2009.5109313.

66 E. Seker, *et al.*, The fabrication of low-impedance nanoporous gold multiple-electrode arrays for neural electrophysiology studies, *Nanotechnology*, 2010, **21**, 125504.

67 Z. Aqrawe, *et al.*, The influence of macropores on PEDOT/PSS microelectrode coatings for neuronal recording and stimulation, *Sens. Actuators, B*, 2019, **281**, 549–560.

68 C. Chiu, X. He and H. Liang, Surface modification of a neural sensor using graphene, *Electrochim. Acta*, 2013, **94**, 42–48.

69 A. Niaraki, *et al.*, Minute-sensitive real-time monitoring of neural cells through printed graphene microelectrodes, *Biosens. Bioelectron.*, 2022, **210**, 114284.

70 M. Hilder, B. Winther-Jensen, D. Li, M. Forsyth and D. R. MacFarlane, Direct electro-deposition of graphene from aqueous suspensions, *Phys. Chem. Chem. Phys.*, 2011, **13**, 9187–9193.

71 J. Wang, L. Min, F. Fang, W. Zhang and Y. Wang, Electrodeposition of graphene nano-thick coating for highly enhanced performance of titanium bipolar plates in fuel cells, *Int. J. Hydrogen Energy*, 2019, **44**, 16909–16917.

72 R. M. Alonso, M. I. San-Martín, A. Sotres and A. Escapa, Graphene oxide electrodeposited electrode enhances start-up and selective enrichment of exoelectrogens in bioelectrochemical systems, *Sci. Rep.*, 2017, **7**, 13726.

73 G. Xiao, *et al.*, Platinum/Graphene Oxide Coated Microfabricated Arrays for Multinucleus Neural Activities Detection in the Rat Models of Parkinson's Disease Treated by Apomorphine, *ACS Appl. Bio Mater.*, 2019, **2**, 4010–4019.

74 Q. Zhang, *et al.*, Synthesis of amphiphilic reduced graphene oxide with an enhanced charge injection capacity for electrical stimulation of neural cells, *J. Mater. Chem. B*, 2014, **2**, 4331–4337.

75 D. Viana, *et al.*, Nanoporous graphene-based thin-film microelectrodes for in vivo high-resolution neural recording and stimulation, *Nat. Nanotechnol.*, 2024, **19**, 514–523.

76 S. Movaghgharnezhad, *et al.*, Neural Electrode Based on 3D Microscale/Nanoscale Porous Graphene Structures for Neural Stimulation, *ACS Appl. Nano Mater.*, 2024, **7**, 23548–23557.

77 N. V. Apollo, *et al.*, Soft, Flexible Freestanding Neural Stimulation and Recording Electrodes Fabricated from

Reduced Graphene Oxide, *Adv. Funct. Mater.*, 2015, **25**, 3551–3559.

78 J. Xiong, *et al.*, Graphene-based implantable neural electrodes for insect flight control, *J. Mater. Chem. B*, 2022, **10**, 4632–4639.

79 M. Deng, *et al.*, Electrochemical deposition of polypyrrole/graphene oxide composite on microelectrodes towards tuning the electrochemical properties of neural probes, *Sens. Actuators, B*, 2011, **158**, 176–184.

80 J. Lin, *et al.*, Laser-induced porous graphene films from commercial polymers, *Nat. Commun.*, 2014, **5**, 5714.

81 N. Dixit and S. P. Singh, Laser-Induced Graphene (LIG) as a Smart and Sustainable Material to Restrain Pandemics and Endemics: A Perspective, *ACS Omega*, 2022, **7**, 5112–5130.

82 R. Ye, D. K. James and J. M. Tour, Laser-Induced Graphene: From Discovery to Translation, *Adv. Mater.*, 2019, **31**, 1803621.

83 Y. Lu, H. Lyu, A. G. Richardson, T. H. Lucas and D. Kuzum, Flexible Neural Electrode Array Based-on Porous Graphene for Cortical Microstimulation and Sensing, *Sci. Rep.*, 2016, **6**, 33526.

84 M. Wang, *et al.*, Nanotechnology and Nanomaterials for Improving Neural Interfaces, *Adv. Funct. Mater.*, 2018, **28**, 1700905.

85 M. Fan, *et al.*, Modified PEDOT by benign preparing N-doped reduced graphene oxide as potential bio-electrode coating material, *Green Chem.*, 2016, **18**, 1731–1737.

86 S. Lee, T. Eom, M.-K. Kim, S.-G. Yang and B. S. Shim, Durable soft neural micro-electrode coating by an electrochemical synthesis of PEDOT: PSS/graphene oxide composites, *Electrochim. Acta*, 2019, **313**, 79–90.

87 G. Filho, *et al.*, All-Polymeric Electrode Based on PEDOT: PSS for In Vivo Neural Recording, *Biosensors*, 2022, **12**, 853.

88 T. D. Y. Kozai, *et al.*, Chronic *In Vivo* Evaluation of PEDOT/CNT for Stable Neural Recordings, *IEEE Trans. Biomed. Eng.*, 2016, **63**, 111–119.

89 Q. Zeng and T. Wu, Enhanced electrochemical performance of neural electrodes based on PEDOT: PSS hydrogel, *J. Appl. Polym. Sci.*, 2022, **139**, 51804.

90 R. Yadav, *et al.*, Intercorrelation between physical and electrochemical behavior of nitrogen-doping in graphene for symmetric supercapacitor electrode, *SN Appl. Sci.*, 2020, **2**, 1630.

91 E. Paek, A. J. Pak, K. E. Kweon and G. S. Hwang, On the Origin of the Enhanced Supercapacitor Performance of Nitrogen-Doped Graphene, *J. Phys. Chem. C*, 2013, **117**, 5610–5616.

92 M. Z. Doğan, D. Gökcen and C. Bayram, Effects of Heteroatom Doping and Physicochemical Character on the Electrochemical Properties of Graphene Sheets, *ChemNanoMat*, 2023, **9**, e202300393.

93 E. Musk and Neuralink, An Integrated Brain-Machine Interface Platform With Thousands of Channels, *J. Med. Internet Res.*, 2019, **21**, e16194.

94 Z. Zhao, *et al.*, Ultraflexible electrode arrays for months-long high-density electrophysiological mapping of thousands of neurons in rodents, *Nat. Biomed. Eng.*, 2022, **7**, 520–532.

95 T. L. Li, *et al.*, Stretchable mesh microelectronics for the biointegration and stimulation of human neural organoids, *Biomaterials*, 2022, **290**, 121825.

96 F. Decataldo, *et al.*, Stretchable Low Impedance Electrodes for Bioelectronic Recording from Small Peripheral Nerves, *Sci. Rep.*, 2019, **9**, 10598.

97 U. A. Aregueta-Robles, A. J. Woolley, L. A. Poole-Warren, N. H. Lovell and R. A. Green, Organic electrode coatings for next-generation neural interfaces, *Front. Neuroeng.*, 2014, **7**, 15.

98 W. Yang, Y. Gong and W. Li, A Review: Electrode and Packaging Materials for Neurophysiology Recording Implants, *Front. Bioeng. Biotechnol.*, 2021, **8**, 622923.

99 A.-I. Lazăr, *et al.*, Graphene-Related Nanomaterials for Biomedical Applications, *Nanomaterials*, 2023, **13**, 1092.

100 D. Convertino, M. L. Trincavelli, C. Giacomelli, L. Marchetti and C. Coletti, Graphene-based nanomaterials for peripheral nerve regeneration, *Front. Bioeng. Biotechnol.*, 2023, **11**, 1306184.

101 V. Lopes, G. Moreira, M. Bramini and A. Capasso, The potential of graphene coatings as neural interfaces, *Nanoscale Horiz.*, 2024, **9**, 384–406.

102 W. Wei and X. Wang, Graphene-Based Electrode Materials for Neural Activity Detection, *Materials*, 2021, **14**, 6170.

103 M. Dong, *et al.*, Graphene-Based Microelectrodes with Reinforced Interfaces and Tunable Porous Structures for Improved Neural Recordings, *ACS Appl. Mater. Interfaces*, 2025, **17**, 9690–9701.